https://doi.org/10.5194/egusphere-2026-4288
Preprint. Discussion started: 14 September 2026

Global fire emissions impact on tropospheric chemistry and radiation in the Energy Exascale Earth System Model (E3SM)

Li Xu[1*], Qi Tang[2], Qing Zhu[3], William J. Riley[3], Guido R. van der Werf[4], Yang Chen[1], Michael J. Prather[1], James T. Randerson[1]

[1]Department of Earth System Science, University of California, Irvine, CA, 92697, USA.
[2]Atmospheric, Earth, and Energy Division, Lawrence Livermore National Laboratory, Livermore, CA 94550, USA.
[3]Earth and Environment Sciences Division, Lawrence Berkeley National Laboratory, Berkeley, California, 94720, USA.
[4]Meteorology and Air Quality Group, Wageningen University and Research, Wageningen, the Netherlands.

Date:
September 7, 2026

[*]Corresponding Author:
Dr. Li Xu
Department of Earth System Science
University of California, Irvine, CA.
Email: lxu16@uci.edu

https://doi.org/10.5194/egusphere-2026-4288
Preprint. Discussion started: 14 September 2026

Abstract

Wildfires release large amounts of trace gases and aerosols into the atmosphere, thereby playing a significant role in structuring tropospheric composition. Understanding and quantifying the interactions between fire, atmospheric chemistry, and climate has become increasingly important as wildfire activity has intensified in many regions over the past several decades. Here, we applied the Energy Exascale Earth System Model (E3SM) version 3, coupled with an interactive chemistry module as its default configuration and GFED5 fire emissions, to assess how contemporary wildfires influence atmospheric composition and radiation. We find that wildfires increase global annual average CO and O_3 column concentrations by 16 ± 2% and 6 ± 1% (reported as mean ± standard deviation hereafter), respectively, during 1997-2022, with the largest increases occurring in wildfire-prone regions of the southern Amazon, central Africa, and tropical Asia. We also find that wildfires strongly promote interannual variations in CO and O_3 at tropical sites, thereby improving consistency with in situ observations. Fire emissions increase global aerosol optical depth (AOD) by 7 ± 2%, resulting in a reduction in net radiation at the surface by about 1.1 W m^{-2}, primarily due to the direct attenuation of incoming solar radiation and indirect cloud effects associated with fire-emitted aerosols. These cooling effects are only partially offset by a small fire-induced ozone radiative warming at surface (+0.07 W m^{-2}). Our analysis provides insight into the spatiotemporal influence of wildfires on global tropospheric trace gas and aerosol abundances and establishes several new diagnostics for evaluating coupled climate-wildfire models.

https://doi.org/10.5194/egusphere-2026-4288
Preprint. Discussion started: 14 September 2026

1. Introduction

Wildfires significantly impact tropospheric composition, affecting the abundances of a wide range of trace gases and aerosol constituents (Akagi et al., 2011; Andreae, 2019; Shahid et al., 2024). Wildfires have long been recognized as playing an important role in shaping tropospheric chemistry (Crutzen and Andreae, 1990) and influencing regional and global climate (Ramanathan et al., 1987) through radiative forcing from changes in methane, ozone, and aerosols (Penner et al., 1992). At a global scale, annual burned area has been estimated to be 774 ± 63 Mha y^{-1} (i.e., 5.9 ± 0.5 % y^{-1} of the global ice-free land surface) over the past three decades, with open savanna ecosystems experiencing a long-term decline as a consequence of agricultural expansion (Andela et al., 2017; Chen et al., 2023). Apart from carbon dioxide (CO_2), other key constituents emitted by wildfires include carbon monoxide (CO), methane (CH_4), nitrogen oxides (NO_x), non-methane volatile organic compounds (VOCs), and primary aerosols of black carbon (BC) and organic carbon (OC). As important sources, fire emissions are responsible for roughly 40% of the global carbon monoxide direct emissions (Olivier et al., 2005; Wiedinmyer et al., 2011; Zheng et al., 2019; Horowitz et al., 2020), 10% to 25% for nitrogen oxides (Oliveira et al., 2007; Horowitz et al., 2020; Jin et al., 2021), 50 to 70% for primary OC aerosol (Bond et al., 2013), and roughly 35-45% for BC (Bond et al., 2013; Feng et al., 2013). Mostly due to VOC and NO_X emissions, wildfires are an important contributor to the formation of tropospheric ozone and secondary organic aerosols through a set of complex photochemical reactions.

Trace gases such as CO_2 and CH_4 are directly emitted from wildfires, and tropospheric ozone is secondarily produced from fire emissions of ozone precursors; together, these gases influence climate as greenhouse gases that absorb the longwave radiation, while tropospheric ozone can also absorb the shortwave solar radiation and alter the heating profile throughout the

https://doi.org/10.5194/egusphere-2026-4288
Preprint. Discussion started: 14 September 2026

atmosphere. Surface ozone damages leaves, thereby reducing photosynthesis and impairing plant productivity (Lombardozzi et al., 2013). Particulate matter and ozone from fire emissions also adversely affect human health by increasing the risk of respiratory problems, cardiovascular diseases, and premature mortality. Johnston et al. (2012) reported that wildfires contribute to as many as 600,000 premature deaths annually worldwide. Recent regional analyses have quantified substantial health burdens associated with extreme wildfire smoke episodes. For example, Zhang et al. (2025) attributed increases in population exposure to hazardous air pollution and a large mortality burden to the 2023 Canadian wildfires; Johnston et al. (2021) estimated hundreds of excess deaths and thousands of smoke-related cardiorespiratory hospitalizations and asthma presentations during the 2019–2020 Australian megafires; and Connolly et al. (2024) reported significant excess mortality and morbidity associated with repeated wildfire smoke events from major California fires between 2008 and 2018.

Wildfire aerosol emissions shape climate through a number of distinct pathways. Key drivers of surface cooling include direct emissions of highly scattering organic aerosol (Penner et al., 1992; Penner et al., 1998; Palm et al., 2020; Szopa et al., 2021; Kelesidis et al., 2025), secondary organic aerosols formed through the condensation of fire-emitted volatile organic compounds (Jimenez et al., 2009; Zhu et al., 2017; Thornhill et al., 2021), and the influence of these aerosols on cloud microphysical properties (Bellouin et al., 2020; Chen et al., 2022). In contrast, fire-emitted black carbon (Ramanathan and Carmichael, 2008; Bond et al., 2013; Coppola et al., 2022) along with large quantities of wildfire-derived brown carbon (Feng et al., 2013; Xu et al., 2026) behave in the opposite manner, strongly absorbing incoming solar radiation and warming the atmospheric layers in which they reside. When black carbon deposits onto snow and ice, it lowers surface albedo and accelerates melting, adding a further warming influence (Flanner et al.,

https://doi.org/10.5194/egusphere-2026-4288
Preprint. Discussion started: 14 September 2026

2007; Skiles et al., 2018; Kang et al., 2020; Réveillet et al., 2022). In Arctic and boreal regions, expected increases in fire aerosols might act as a negative feedback on climate warming, as a consequence of regional decreases in surface solar radiation and surface air temperature, further amplified by decreases in sea ice loss (Blanchard-Wrigglesworth et al., 2025). Beyond the balance between aerosol absorption and scattering, post-fire increases in surface albedo within fire perimeters may further offset warming caused by fire emissions of greenhouse gases (van Gerrevink et al., 2026).

Investigating the impacts of fire emissions on chemistry-climate interactions typically relies on an Earth System Model (ESM) or a chemistry-climate model. Examples of ESMs with comprehensive atmospheric chemistry, including interactive ozone in both the troposphere and stratosphere, are UKESM1 (Archibald et al., 2020), GFDL-AM4.1 (Horowitz et al., 2020), CESM2 (Gettelman et al., 2019; Emmons et al., 2020). In particular, ESMs that include interactive chemistry mechanisms provide a more comprehensive representation of atmospheric composition and its spatial and temporal variability. For instance, Mao et al. (2013) investigated the sensitivity of tropospheric oxidant concentrations to fire emissions using the GFDL-AM3 chemistry-climate model. Gaubert et al. (2016) used the CESM1.2 chemistry-climate model to evaluate CO emissions and their impact on tropospheric composition. Xie et al. (2022) studied western US surface fine particle concentration (i.e., PM2.5) changes from wildfires in a warming climate using the GFDL ESM4.1 global model with interactive stratosphere-troposphere chemistry.

In addition to better representing the spatial distribution and temporal variability of atmospheric constituents, ESMs with chemistry-climate coupling can capture feedbacks among atmospheric chemistry, atmospheric dynamics, and other components of the Earth system such as atmosphere-land interactions. For example, using CESM2, Fasullo et al. (2023) showed that

https://doi.org/10.5194/egusphere-2026-4288
Preprint. Discussion started: 14 September 2026

aerosol emissions from the Australian wildfires during the 2019-2020 dry season contributed to decreases in absorbed shortwave radiation across the Southern Hemisphere, which, in turn, through atmosphere-ocean teleconnections, likely intensified surface cooling and the concurrent La Niña state across the tropical Pacific.

Here, we explore the impacts of fire emissions on tropospheric chemistry and radiation using the Energy Exascale Earth System Model version 3 (E3SMv3). E3SMv3 includes interactive chemistry in its default configuration (Tang et al., 2025). We performed two global simulations using E3SMv3 with and without fire emissions prescribed from the Global Fire Emissions Database version 5 during 1997-2022. The data and methods are described in Section 2, along with satellite and in situ observations used for model evaluation. We report the influence of wildfires on OH, CO, and O_3 concentrations; aerosol optical depth; and atmospheric radiation in Section 3, and compare these results with available observations. We discuss the indirect effect of wildfires on the CH_4 lifetime through changes in OH in Section 4, along with implications from our analysis for the evaluation of prognostic wildfire simulations. We provide a brief summary and conclusions in Section 5.

2. Data and Methods

2.1 Energy Exascale Earth System Model

We used the Energy Exascale Earth System Model version 3 (E3SMv3) (Xie et al., 2025) and its default interactive chemistry (Tang et al., 2025) to simulate the influence of wildfires on atmospheric chemistry constituents. The new chemistry submodel includes the chemUCI interactive tropospheric package (Prather and Zhu, 2024b) and the Linoz version 3 interactive stratospheric package (Hsu and Prather, 2010). The chemUCI submodel in the troposphere

https://doi.org/10.5194/egusphere-2026-4288
Preprint. Discussion started: 14 September 2026

implements 28 advected tropospheric tracers and solves for more than 80 chemical reactions of the O_3-CH_4-HO_x-NO_x-NMVOCs chemistry. In the stratosphere, the Linoz v3 module calculates four prognostic gas tracers (O_3, CH_4, N_2O and NO_Y) with a first-order Taylor expansion around a monthly zonal mean climatology of ozone column and local values of O_3, CH_4, N_2O, NO_Y, and temperature (Hsu and Prather, 2010). The chemistry module alters the radiative forcing of the E3SM model by calculating 3-D fields of stratospheric and tropospheric O_3 and stratospheric H_2O, CH_4 and N_2O every time step. The radiative transfer calculations have been evaluated for both their chemistry and climate response in Tang et al. (2025).

In our analysis, we used the default configuration of E3SMv3 (Xie et al., 2025), which has a horizontal resolution of about 1° × 1° and 80 vertical layers extending from the Earth's surface to about 0.1 hPa. The E3SM atmospheric model (EAM) uses a spectral element dynamical core (Taylor and Fournier, 2010; Dennis et al., 2012) on a cubed-sphere computational grid. The aerosol module used in E3SM is an updated 5-mode version of the modal aerosol module (MAM5) with prognostic stratospheric sulfate (Hu et al., 2025). In E3SM version 3, the atmospheric chemistry and aerosol modules are implemented as separate components, with chemistry calculations performed independently of the aerosol module.

We performed two E3SM simulations to examine the impacts of wildfires on trace gases and aerosols (Table 1): (1) we included the history of GFED5 fire emissions of trace gases and aerosols during 1997-2022 (i.e., the control simulation) and (2) we excluded all GFED5 emissions (i.e., the no-fire simulation). In both simulations, we used the same non-fire emissions of trace gases and aerosols from anthropogenic (Hoesly et al., 2018) and biogenic sources (Sindelarova et al., 2014). Sea surface temperatures (SSTs) were prescribed as the ocean surface boundary condition in all of the simulations using the Hadley Center monthly mean sea surface temperature

https://doi.org/10.5194/egusphere-2026-4288
Preprint. Discussion started: 14 September 2026

dataset merged with version 2 of the National Oceanic and Atmospheric Administration (NOAA) weekly optimum interpolation sea surface temperature analysis (Hurrell et al., 2008). The monthly and annual variations in SSTs over the 1997-2022 period enable the model to partially capture the influence of El Niño and other climate modes on large-scale atmospheric dynamics.

2.2 Fire emission inventory

We used emissions of trace gases, primary carbonaceous (i.e., black carbon and organic matter) and sulfate aerosols, and precursor gases for secondary organic aerosols and SO_2 from the Global Fire Emissions Database, version 5 (GFED5) (van der Werf et al., 2025). The GFED5 emissions inventory covers 1997-2022 at a spatial resolution of 0.25°×0.25° and a monthly temporal resolution.

Global annual mean fire emissions for the 1997-2022 period, along with standard deviations computed from year-to-year variability, are reported in Table 2. Averaged over this period, wildfires emitted 529.7 Tg y^{-1} of CO, 41.0 Tg y^{-1} of non-methane hydrocarbons (NMHCs), 24.3 Tg y^{-1} of NO, and 5.9 Tg y^{-1} of SO_2. The wildfire relative contribution to the direct emissions of non-methane hydrocarbon gases ranged from 0.2% for isoprene to 60% for CH_2O. Over the study period, the GFED5 inventory emitted 19 Tg CH4 y^{-1}. This source was not used because in our simulations, CH_4 is interactively diagnosed in the stratosphere and reacts with OH in the troposphere, relaxing towards observations at the surface (Tang et al., 2025). Mean wildfire aerosol emissions during this period were estimated to be 38 Tg y^{-1} for POM (73% of total emissions) and 2.5 Tg y^{-1} for BC (37% of the total). We assumed that all primary sulfate aerosol emissions were in the form of ammonium bisulfate, with a total mass estimated at 2.5% of fire SO_2 emissions (Liu et al., 2012). The new GFED5 emissions are substantially greater than earlier versions of the GFED inventory for most species, reflecting markedly increased burning in savanna, grassland, and

https://doi.org/10.5194/egusphere-2026-4288
Preprint. Discussion started: 14 September 2026

agricultural ecosystems, driven by improved burned-area mapping using higher-resolution satellite imagery. The improved burned area estimates provide a renewed opportunity to reassess the influence of fires on atmospheric chemistry and radiative forcing. Within the E3SMv3 emissions framework, wildfires account for approximately 47% of global CO emissions, 22% of NO emissions, and 5% of SO_2 emissions (Table 2). Following the standard configuration of E3SMv3, fire-emitted aerosols are injected into the atmosphere using a mean injection profile derived for each of the 14 continental regions using MISR observations (val Martin et al., 2018) described in Xu et al. (2021).

In E3SM version 3, secondary organic aerosols (SOAs) are represented using a modified Volatility Basis Set (VBS) approach that applies to both SOA precursor gases and particulate SOAs (Shrivastava et al., 2015; Lou et al., 2020). The semi-volatile and intermediate volatility SOA precursor gases (S/IVOC) emitted from wildfire, biofuel, and fossil fuel sources are scaled with the traditional primary organic aerosol (POA) inventory co-emitted from the same sources, which has been widely adopted in the SOA modeling community. The IVOC-to-POA mass ratio is a critical parameter in regional and global atmospheric models, used to account for unspeciated gas-phase IVOCs co-emitted with POA but missed by traditional emission inventories. For instance, the most widely adopted value is 1.5 in regional (Koo et al., 2014) and global models (Hodzic et al., 2010; Jathar et al., 2011), a convention derived from observations from diesel-exhaust smog-chamber studies by Robinson et al. (2007) and Grieshop et al. (2009). This ratio can vary widely, with some studies reporting IVOC-to-POA ratios exceeding 1.5. For example, Shrivastava et al. (2015) assume that S/IVOC emissions were 6.5 times those of POA from biomass burning and fossil fuels. Lou et al. (2020) assumed that IVOC emissions were 4 times POA emissions because the simulated organic aerosol concentrations and aerosol optical depth

https://doi.org/10.5194/egusphere-2026-4288
Preprint. Discussion started: 14 September 2026

yielded a better agreement with available observations for the E3SMv1 model. Tsimpidi et al. (2010) adopted a factor of 3.0 for anthropogenic sources in a three-dimensional chemical transport model (i.e., PMCAMx). The wide range of this ratio highlights a key uncertainty in the SOA modeling. Here we adopted 1.5, recommended by Robinson et al. (2007) and Grieshop et al. (2009), as a baseline to maintain consistency with the mass budget of non-methane hydrocarbon trace gas emissions. With this assumption, emissions of the initial secondary organic aerosol precursor gas (i.e., SOAG0 in Table 2) are estimated to be 57 Tg y^{-1} for wildfires, about 53% of the 107 Tg y^{-1} of non-methane hydrocarbon emissions reported in GFED5 (van der Werf et al., 2025). This allows for consistency with observations that direct oxidation (to CO and CO_2) of many non-methane hydrocarbon species with lower SOA-forming potential is also an important loss pathway (Hatch et al., 2017). Compared with anthropogenic sources of SOAG0, wildfires contribute about 68% of the total global emissions.

2.3 Anthropogenic emission inventory

We applied an updated global anthropogenic emission inventory of reactive gases and aerosols from the v2025_04_18 version of Community Emission Data System (CEDS) (Hoesly et al., 2018), which covers the period 1750-2023. This CEDS dataset includes monthly anthropogenic emissions of primary organic matter, black carbon, sulfate, and SO_2 with updated seasonality including sub-annual variations during COVID. The detailed description of the up-to-date CEDS data is accessible at https://github.com/JGCRI/CEDS. Other greenhouse gas mole fractions, including CO_2, N_2O, CFC11, and CFC12, were prescribed annually and evolved with time. Emissions of dust and sea salt aerosols were calculated online as a function of wind speed and temperature.

2.4 Observations for model evaluation

https://doi.org/10.5194/egusphere-2026-4288
Preprint. Discussion started: 14 September 2026

To evaluate the tropospheric CO column from model simulations, we used the Measurement of Pollution in the Troposphere (MOPITT) v9 gridded monthly mean product (Deeter et al., 2021). We used the MOPITT monthly mean averaging kernels with our modeled data for this comparison, following the MOPITT Version 9 Product User's Guide. We also compared model-simulated surface CO with measurements from four representative stations across different latitude belts in the Carbon Cycle Greenhouse Gases (CCGG) Cooperative Air Sampling Network maintained by the Global Monitoring Laboratory (GML) of the National Oceanic and Atmospheric Administration (NOAA) (https://gml.noaa.gov/ccgg/data/co.html). The four selected sites were: 1) Utqiaġvik (formerly Point Barrow), AK, USA; 2) Mauna Loa, Hawaii, USA; 3) Ascension Island, UK; and 4) South Pole, Antarctica, USA. Monthly mean surface CO mole fractions from 1997 through 2022 were used to evaluate model performance.

To evaluate modeled tropospheric O_3, we use the monthly gridded troposphere column ozone derived for 60°S-60°N from the Aura Ozone Monitoring Instrument/Microwave Limb Sounder (OMI/MLS) (Ziemke et al., 2006) for the January 2005-December 2020 period. The modeled monthly mean total column ozone values were compared directly with the OMI/MLS product; no adjustments were applied to account for differences in clear-sky and cloudy-sky sampling that have the potential to influence the satellite retrievals. In E3SM, total column ozone was diagnosed at each model time step for every atmospheric column using a tropopause height determined from the e90 tracer following Prather (2025).

To evaluate surface ozone, we selected several stations in the Tropospheric Ozone Assessment Report (TOAR) database (https://toar-data.org/surface-data/) where wildfires were major sources of air pollution and the observed time series had sufficient duration to enable comparisons on seasonal and interannual timescales. The six representative sites were a) Utqiaġvik,

https://doi.org/10.5194/egusphere-2026-4288
Preprint. Discussion started: 14 September 2026

AK, USA (formerly Point Barrow), b) Cape Verde, Africa, c) Huancayo, Peru, d) American Samoa, USA, e) Cape Grim, Australia, f) South Pole, Antarctica, USA. We computed the monthly mean ozone using the 24-hour mean data for each site.

To evaluate aerosol optical depth (AOD), we compared the monthly-averaged AOD from E3SM with satellite retrievals from the monthly Level-3 MODIS-Terra product MOD08_M3, Collection 6.1 (Sayer et al., 2014).

3. Results

3.1 The influence of fires on atmospheric composition

3.1.1 OH

Tropospheric hydroxyl radical, OH, determines the oxidizing potential of the troposphere and controls the lifetime of CH_4, CO, NO_x, and various other non-methane hydrocarbon gases relevant for climate and air quality. Figure 1a shows the geographic distribution of column-averaged annual-mean OH concentration over the years 1997 through 2022. Our E3SM-simulated tropospheric mean OH concentration of 11.1×10^5 molecules cm^{-3} is slightly greater than the value of 10.7×10^5 molecules cm^{-3} reported by Tang et al. (2025), but our simulation includes updated anthropogenic and wildfire emissions. Our value falls within the multi-model range of 8.7×10^5 to 12.8×10^5 molecules cm^{-3} reported by Zhao et al. (2019) and is consistent with their geographic pattern.

The influence of wildfires on tropospheric column-mean OH concentrations is complex. Wildfires increase OH by 10–20% in high-fire regions of South America, central Africa, and tropical Asia, where elevated NO_x emissions from fires, together with abundant sunlight and water vapor, favor the OH formation. In contrast, fires decrease OH concentrations in remote oceanic

https://doi.org/10.5194/egusphere-2026-4288
Preprint. Discussion started: 14 September 2026

and polar regions (Fig. 1b). This spatial pattern reflects a short-lived enhancement of OH near source regions driven by wildfire-emitted NO_x, alongside a more widespread reduction in the remote troposphere due to OH loss by fire-emitted CO. The resulting 3.7 ± 1.7% global decline in OH implies a modest lengthening of the atmospheric CH_4 lifetime, an effect examined further in Section 4.2. The mean reported here is for the 1997-2022 period, and the standard deviation is estimated from the year-to-year variability given in Table 2. The direction of the mean global OH change is consistent with simulations from the fully coupled Earth system model GFDL-AM3, which report an approximately 6% decline attributable to fire emissions (Mao et al., 2013).

3.1.2 CO

To explore the influence of wildfire on the column CO abundance, we compared our model simulations with MOPITT retrievals (Figure 2). The simulated spatial pattern of the tropospheric CO column from the control simulation with fire emissions included agrees reasonably well with the MOPITT retrievals in terms of magnitude and spatial distribution. The simulated global mean CO column of 15.3 ± 1.3 $\times 10^{17}$ molecules cm^{-2} for 2000-2022 is approximately 5% lower than the MOPITT estimate. However, the control simulation underestimates CO in mid- and high-latitude regions of the Northern Hemisphere and slightly overestimates CO in the Southern Hemisphere (Figure 3a), thereby improving the column CO underestimates over the whole globe relative to the no-fire simulation (Figure 3b). A similar hemispheric model bias in simulating the tropospheric CO column is reported by Horowitz et al. (2020) for the GFDL-AM4.1 fully coupled ESM. The relative influence of wildfires on the column CO is greater in tropical and boreal forest areas, whereas it is lower in Northern Hemisphere temperate regions, because the background CO column is typically higher owing to larger anthropogenic emissions there (Figure 2c). Wildfires contribute to a 16 ± 2% increase in global mean column CO, with the largest relative increases of

https://doi.org/10.5194/egusphere-2026-4288
Preprint. Discussion started: 14 September 2026

over 30% centered in wildfire-prone regimes, including central Africa and boreal forest ecosystems across North America and Eurasia (Figure 2d).

In the historical record, large but infrequent wildfire complexes have generated extensive CO plumes that persist for weeks to months and disperse across downwind continental regions and adjacent ocean basins. The long atmospheric lifetime of CO, together with observations of fire-specific emission factors, has enabled atmospheric inversion studies to estimate carbon emissions from major wildfire events (Byrne et al., 2024; Zheng et al., 2023; van der Velde et al., 2021; Liu et al., 2017; van der Werf et al., 2004). Here, we examine the influence of the timing and magnitude of wildfire-driven CO anomalies on CO column observation as an independent benchmark for model evaluation (Figure 4). Including fire emissions considerably improves both the correlation (Figures 4a and 4b; Table 3) and the ratio of standard deviations of interannual CO anomalies from the model relative to the MOPITT observations (Figures 4c and 4d), highlighting the widespread and persistent influence of wildfire emissions on tropospheric CO in remote regions far away from high-fire source regions. This comparison tests the model's ability to represent the transport, dispersion, and chemical evolution of large fire-emission plumes. In addition to the interannual variability signal captured by the MOPITT CO column anomalies, fire emissions substantially improve the spatial agreement between the simulated and observed annual mean column CO from MOPITT, increasing the spatial correlation from 0.75 in the no-fire simulation to 0.88 in the control simulation, and yielding even greater improvements when considering the mean annual cycle and the full time series (Table 3).

In the tropics, fire emissions are critical for explaining seasonal and interannual variability of column CO over continental regions (Figure 5). The simulated column CO time series during 2000-2022 from the control simulation for all three tropical regions shows much better agreement

https://doi.org/10.5194/egusphere-2026-4288
Preprint. Discussion started: 14 September 2026

with the MOPITT observations than the no-fire simulation, with correlations of 0.93, 0.83, and 0.84 for the control simulation and 0.46, -0.07, and -0.02 for the no-fire simulations in the southern Amazon, central Africa, and tropical Asia, respectively (Figures 5a-5c, Table 4). In the southern Amazon and tropical Asia, E3SM captures both the magnitude and seasonal timing of monthly peaks in MOPITT column CO, as well as interannual variability over the 23-year period. In central Africa, the simulation that includes fire emissions significantly improves the representation of seasonal and interannual variation in column CO, whereas the no-fire simulation misses the observed semiannual cycle (Figure 5b, Table 4). In tropical Asia, including fire emissions improves the model's ability to capture El Niño-driven positive emissions anomalies associated with peat burning, as observed by MOPITT in 2002, 2006, 2015, and 2019.

Comparisons between simulated surface CO concentrations and observations from NOAA GML monitoring sites further reveal a persistent underestimation of CO concentrations in the Northern Hemisphere. At Utqiaġvik in Alaska (formerly Point Barrow), inclusion of fire emissions brings E3SM's annual mean CO concentrations into closer agreement with observations but degrades the model's ability to reproduce the magnitude and phase of the seasonal cycle (Fig 6a). In contrast, at Mauna Loa, Ascension Island, and the South Pole, the control simulation improves the simulation of both the annual mean and the seasonal cycle of CO (Figs. 6b–6d). At Ascension Island in particular, the seasonal variability in CO is dominated by fire emissions, indicating that this site—located in the outflow from southern Africa—may provide a strong constraint on long-term trends in burned area and fire emissions from the region. Similarly, nearly half of the annual mean CO cycle at the South Pole originates from fire emissions, suggesting that this station may be valuable for constraining interannual variability and trends in the integrated sum of fire emissions across the Southern Hemisphere.

https://doi.org/10.5194/egusphere-2026-4288
Preprint. Discussion started: 14 September 2026

3.1.3 O_3

Tropospheric ozone, which is secondarily produced from fire emissions of NO_x and hydrocarbons, is a key atmospheric constituent that influences radiative forcing of the climate (Szopa et al., 2021). We evaluated simulated annual mean tropospheric ozone columns against satellite-based estimates from the OMI/MLS instruments (Ziemke et al., 2019). Over 2005–2020, the global mean simulated tropospheric ozone column within 60°S–60°N is approximately 30.3 ± 0.4 Dobson Units (DU), about 3% lower than the OMI/MLS mean value of 31.4 ± 0.9 DU and likely within the combined observational and modeling uncertainties (Figs. 7a and 7b). The model exhibits localized overestimations in high-fire areas such as the southern Amazon and central Africa. Fire emissions substantially increase tropospheric ozone, enhancing global mean columns by approximately 6 ± 1% (Figs. 7c and 7d). This response is consistent with prior estimates that attribute about 3.5% of global tropospheric ozone to fire emissions (Jaffe and Wigder, 2012). Including fire emissions slightly reduces correlations with OMI/MLS observations in spatial, climatological mean annual cycle, and full time series comparisons (Table 3). However, when considering monthly anomalies and the influence of fires on interannual variability of ozone, the inclusion of fire emissions slightly improves model agreement, suggesting systematic bias in the annual mean climatology. The largest relative increase in tropospheric ozone columns—exceeding 20% (i.e., 8 DU in absolute difference terms in Fig. 7c)—occurs in central Africa, highlighting the strong influence of wildfire activity in Africa on regional ozone burdens and a possible high bias in NO_x or non-methane hydrocarbon emissions from savanna ecosystems.

Time-series comparisons with OMI/MLS observations indicate that the positive biases in the model O_3 tropospheric column in high fire regions are persistent on annual and interannual timescales, and that fire emissions exacerbate these biases across all three tropical continents

https://doi.org/10.5194/egusphere-2026-4288
Preprint. Discussion started: 14 September 2026

(Figure 8). For the southern Amazon, including fire emissions increases the positive bias, but considerably improves the representation of the column O_3 annual cycle, shifting the phase to match the observed peak in October, near the end of the dry season. In central Africa and tropical Asia, improvements in the phasing of the annual cycle from the inclusion of fire emissions were modest, and over central Africa, fire emissions contributed to an annual cycle approximately a factor of two larger than the observations.

Comparison of model-simulated O_3 mole fractions with observations from the NOAA Global Monitoring Laboratory (GML) and the Tropospheric Ozone Assessment Report (TOAR) networks indicates that fire emissions exert only a weak influence on surface O_3 in remote regions (Figure 9). At Utqiaġvik, Cape Verde, American Samoa, Cape Grim, and the South Pole (Figs. 9a-9b, 9d-9f), the E3SM control and no-fire simulations are nearly indistinguishable. In contrast, at Huancayo, Peru—located on the eastern flank of the Andes—fire emissions substantially improve the simulated O_3 magnitude and seasonal cycle (Figure 9c). The influence of fire on the annual cycle at this Amazon basin site is consistent with its impact on tropospheric column O_3 over the southern Amazon (Figure 8a). At Utqiaġvik, the model substantially overestimates surface O_3 during late winter and spring (Figure 9a). Although this bias shows little sensitivity to fire emissions, it may reflect the absence of halogen chemistry in the current E3SM chemical mechanism or biases in simulated stratosphere–troposphere exchange.

3.2 The influence of wildfires on aerosol optical depth and atmospheric radiation

To assess the influence of wildfires on the atmospheric radiation budget, we first examined the simulated global mean total AOD and compared it with observations from MODIS. The global annual mean AOD in the control simulation is 0.10 for 2000–2022, comparable to the value of 0.11 reported for 2000–2014 by Xie et al. (2025), but substantially lower than the MODIS-derived

https://doi.org/10.5194/egusphere-2026-4288
Preprint. Discussion started: 14 September 2026

mean of 0.17 (Figures 10a and 10b). The control simulation exhibits a systematic low bias over eastern Asia, northern Africa, South America, and across many remote ocean regions. Both the sign and magnitude of this bias are broadly consistent with the low AOD biases reported by Xie et al. (2025) for E3SMv3 when evaluated against AERONET AOD and surface observations of sulfate (SO_4) and black carbon (BC).

The influence of fire aerosols on AOD is strongest in tropical and boreal regions. Annual mean AOD regional enhancements attributable to fire emissions exceed 0.05—corresponding to relative increases of more than 30%—across central and southern Africa, the southern Amazon, Southeast Asia, and extensive boreal regions of North America and Eurasia (Figures 10c and 10d). Globally, fire aerosol emissions increase mean AOD by approximately 7 ± 2% (Figure 10d). Including fire emissions in the model substantially improves both the spatial and temporal correlations with MODIS AOD observations (Table 3).

Time-series comparisons between E3SMv3 and MODIS AOD over tropical continental regions demonstrate that fire emissions are essential for reproducing both the seasonal cycle and the interannual variability of AOD. Across tropical Asia, the southern Amazon, and central Africa, the control simulation consistently exhibits higher temporal correlations and lower root-mean-square errors (RMSE) than the no-fire simulation (Figure 11, Table 4). In tropical Asia, the model captures observed AOD maxima in 2002, 2006, 2015, and 2019, with corresponding peaks in the southern Amazon occurring approximately one year later. This phasing is consistent with previous studies showing that El Niño events initiate a cascading sequence of enhanced wildfire activity across tropical regions (Chen et al., 2017). In central Africa, inclusion of fire emissions is particularly important for reproducing the observed semiannual AOD cycle, which is largely absent in the no-fire simulation.

https://doi.org/10.5194/egusphere-2026-4288
Preprint. Discussion started: 14 September 2026

The direct and indirect radiative effects of carbonaceous aerosols, particularly those emitted by landscape fires, interact in complex ways with Earth's radiation balance. Primary organic matter and secondary organic aerosols generated from wildfires primarily act as scattering aerosols, increasing the reflectance of shortwave radiation at the top of the atmosphere and thereby reducing the downward shortwave radiation flux reaching the surface. In contrast, black carbon plays an important role in atmospheric warming but can also attenuate surface solar radiation through absorption and scattering. Figure 12 shows the spatial distribution of wildfire-induced aerosol direct and indirect effects on radiation at the surface and the top of the atmosphere. The global average net aerosol direct effect from fire emissions at the surface is about -0.8 ± 0.1 W m^{-2} (Figure 12a), contributing to a net cooling effect at the surface (Xu et al., 2021). Wildfire aerosols exert nearly zero change in net radiation at the top of the atmosphere (Figure 12b). Moreover, the fire aerosol indirect effect, stemming from the influence of fire aerosols on cloud properties, leads to an additional small negative change in both surface and top-of-atmosphere radiative fluxes (-0.4 ± 0.3 W m^{-2}) shown in Figure 12c and 12d. Notably, the regional impact of this indirect effect is most pronounced in central and western Africa, coinciding with the influence of the direct effect in these areas (Figures 12c and 12d).

In addition to the radiative perturbation from fire-emitted aerosols, the fire-enhanced tropospheric O_3 (shown in Figure 5) absorbs more incoming solar radiation, resulting in a small warming radiative effect of +0.02 ± 0.01 W m^{-2} at the surface and at TOA, with the largest increase of more than +0.3 W m^{-2} in central Africa shown in Figure 13a and13b. At the same time, tropospheric O_3 serves as a potent greenhouse gas that efficiently absorbs infrared radiation, leading to a positive longwave radiative effect of +0.05 ± 0.04 W m^{-2} at the surface with the maximum increases over +0.3 W m^{-2} in central Africa (Figure 13c). The longwave radiative effects

https://doi.org/10.5194/egusphere-2026-4288
Preprint. Discussion started: 14 September 2026

display a relatively smaller magnitude of +0.03 ± 0.02 W m^{-2} at the TOA (Figure 13d) because the fire-enhanced O_3 layer mainly resides in the warm lower troposphere close to the surface. Together, the global mean net radiative effect at TOA from fire-induced ozone increases, including both shortwave and longwave components, is +0.05 ± 0.04 W m^{-2}, consistent with the approximately +0.03 W m^{-2} effect attributable to fire emissions from the fully coupled Earth system model GFDL-AM3 (Mao et al., 2013).

In response to both aerosol direct and indirect effects, surface solar radiation over land decreases by 1.2 W m^{-2} (1.6%) in the control simulation relative to the no-fire simulation. The overall fire aerosol direct and indirect effect is smaller than those reported in Xu et al. (2021), likely as a consequence of the negative aerosol bias in E3SMv3, even though fire emissions of particulate matter in GFED5 are about 60% higher (van der Werf et al., 2025). With the additional fire-enhanced tropospheric O_3 positive radiative effects in both shortwave and longwave spectra, fire emissions contribute a net radiative effect (shortwave and longwave) of about -1.12 W m^{-2} at the surface. At TOA, the decreases in shortwave radiative effects due to fire aerosols are partially offset by the warming effects due to fire-enhanced tropospheric O_3, resulting in a net radiative effect of -0.35 W m^{-2} at TOA.

4. Discussion

4.1 Indirect effect of fires on the CH_4 lifetime

Interactions between atmospheric OH and CH_4 significantly amplify the impacts of fire emissions on CH_4 interannual variability and trends. Specifically, increases in fire-emitted CO and CH_4 reduce tropospheric OH, thereby extending the CH_4 lifetime and enhancing its overall atmospheric abundance, which has been identified as a positive climate-carbon cycle feedback in

https://doi.org/10.5194/egusphere-2026-4288
Preprint. Discussion started: 14 September 2026

past work (Chen et al., 2026). As reported in Section 3.1 above, wildfires overall reduce global OH concentrations by 3.7%. Assuming a background mean CH_4 concentration of 1805 ppb during 1997-2022 (Dlugokencky et al., 1994) and assuming a CH_4 tropospheric chemical lifetime with respect to OH of 11.2 years constrained by methyl chloroform surface observations (Prather et al., 2012), global fire emissions generate about 16.5 Tg CH_4 y^{-1} assuming a conversion factor of 2.748 Tg CH_4 ppb^{-1} (Prather et al., 2012), through fire emission impacts on OH. This indirect effect is comparable to the direct annual mean fire CH_4 emissions of 18.7 ± 3.4 Tg CH_4 y^{-1} estimated by GFED5 (Table 2).

4.2 Steps toward reducing uncertainties in future ESM assessments of fire impacts

Our analysis highlights several priorities for model improvement, spanning both the fire emissions inventory and the representation of atmospheric chemistry and aerosols in the Earth system model. The persistent high biases in CO and O_3 column abundances over central Africa (Figures 5 and 8) suggest that GFED5 may overestimate savanna fire emissions in northern and southern Africa. Emissions from this biome increased by approximately 70% from GFED4 to GFED5, primarily due to the incorporation of 20 m Sentinel-2 burned-area estimates to correct omission and commission errors in the 500 m MODIS burned-area product that serves as the primary reference dataset for the time series. As burned area estimation from Sentinel-2 and Landsat time series continues to improve in quality and expand in scope, further refinements in burned-area mapping and associated emission estimates are expected. Evidence for a positive emission bias also emerges in boreal forests of North America and Eurasia. At Utqiaġvik, the coupled simulation shows a weaker annual CO cycle than observations, implying that simulated summer fire emissions may be too large. In this region, enhanced summertime emissions offset CO losses from faster chemical removal, and the model–observation mismatch suggests this

https://doi.org/10.5194/egusphere-2026-4288
Preprint. Discussion started: 14 September 2026

compensating effect is overestimated. A key remaining uncertainty in boreal emission estimates concerns how low-severity burns are treated and how well GFED5 represents fuel consumption in these areas.

Within E3SM, the pervasive negative bias in AOD in the control simulation indicates that aerosol removal processes—particularly dry and wet deposition—and other aspects of aerosol parameterization require further evaluation and optimization. The magnitude and spatial structure of the negative AOD bias are consistent with AERONET and surface network comparisons reported for E3SMv3 by Xie et al. (2025). Notably, this bias persists across regions and time periods characterized by both active and minimal fire influence. For example, in tropical Asia, simulated AOD during La Niña conditions—when elevated precipitation suppresses fire activity—is more than a factor of two lower than MODIS observations, as shown in Figure 11c. This pattern suggests that processes unrelated to fire emissions contribute substantially to the model–observation discrepancies. It is also important to apply more advanced algorithms to dynamically account for the injection height of fire aerosol emissions in the atmospheric model. Recent extreme wildfire events in Australia, California, and Canada have produced pyrocumulonimbus (pyroCb) convection, lofting aerosols into the upper troposphere and lower stratosphere and thereby substantially increasing aerosol lifetimes and radiative impacts (Peterson et al., 2021). Although individual pyroCb events have been simulated in E3SM using regionally refined grids and a multiscale modeling framework (Ke et al., 2025), a critical next step is to develop a systematic capability to identify and represent these events in multi-year global simulations.

The underestimation of surface CO concentrations in E3SM relative to observations over the boreal northern hemisphere is a persistent bias reported in multiple global modeling studies (Alvarado et al., 2010; Hooghiemstra et al., 2012; Mao et al., 2013; Tang et al., 2025). This model–

https://doi.org/10.5194/egusphere-2026-4288
Preprint. Discussion started: 14 September 2026

observation discrepancy likely reflects biases in atmospheric chemistry and transport, uncertainties in anthropogenic emissions, or limitations in surface station data used for evaluation (Bian et al., 2007). Mao et al. (2013) demonstrated that excessive tropospheric OH in models can lead to systematic CO underestimation. Hooghiemstra et al. (2012) suggested that anthropogenic emissions from Asia may be too low to reproduce observed Northern Hemisphere CO levels, while Alvarado et al. (2010) identified chemical and transport adjustments needed to reduce high-latitude CO biases. van Leeuwen et al. (2013) reported that model–observation discrepancies in surface CO exceeded differences among wildfire emission inventories, underscoring the dominant role of chemical and transport processes. Tang et al. (2025) also found a systematic CO underestimation in E3SM-chem over the Northern Hemisphere and attributed it to underestimated CO and VOC precursor emissions.

Taken together, these studies indicate that CO biases in northern high latitudes likely arise from a combination of emissions biases and errors in chemical processing. A systematic negative bias in boreal wildfire emission inventories appears unlikely to be the dominant factor, particularly given the remaining challenges in accurately reproducing the observed seasonal cycle shown in Figure 6. Instead, low biases in CO emitted by fossil fuel sources or uncertainties in OH chemistry may play a more central role. Refinements in the representation of OH—such as improved treatment of radiation absorption by water vapor (Prather and Zhu, 2024a) and reductions in background aerosol biases described above—could decrease simulated OH concentrations and thereby increase CO lifetimes.

4.3 Toward a wildfire emissions benchmark

Our analysis provides a first step toward developing a systematic framework for benchmarking fire emissions and their atmospheric impacts in Earth system models. By comparing

https://doi.org/10.5194/egusphere-2026-4288
Preprint. Discussion started: 14 September 2026

simulations with and without fire emissions while prescribing observed sea surface temperatures, our experimental design allowed us to isolate the contribution of fires to seasonal and interannual variability in carbon monoxide, ozone, and aerosol optical depth. These model–observation comparisons demonstrate the important role of fire emissions in regulating atmospheric composition, particularly in column observations over tropical continents and at surface stations downwind of major fire regions.

Several extensions will be needed to develop a more comprehensive benchmarking framework. First, the analysis could incorporate a broader suite of observational constraints, including column measurements of carbon monoxide and NO_x from Tropospheric Monitoring Instrument (TROPOMI) (van der Velde et al., 2021; Jin et al., 2021), column carbon dioxide from Orbiting Carbon Observatory-2 (OCO-2) (Liu et al., 2017), and surface PM2.5 observations (Zhang et al., 2023). Second, automating model–observation comparisons across a larger and more representative set of locations and stations would enable systematic evaluation across fire regimes, chemical environments, and downwind regions. Third, complementary benchmarks are needed for fully coupled Earth system model simulations, in which the timing of individual climate extremes and fire events is not expected to coincide with the observed record. Such benchmarks could instead evaluate whether models reproduce observed relationships between fire emissions, atmospheric composition, and large-scale modes of climate variability, including the El Niño–Southern Oscillation. An important next step is to apply this framework to the fully coupled fire model in E3SMv3. Comparing simulated fire emissions and their atmospheric impacts against these observational benchmarks will provide a quantitative assessment of model performance and help identify biases in fire activity, emissions, and atmospheric responses before using E3SMv3 to investigate coupled fire–climate interactions.

https://doi.org/10.5194/egusphere-2026-4288
Preprint. Discussion started: 14 September 2026

5. Conclusions

Here, we used E3SMv3 with interactive atmospheric chemistry to quantify the influence of fire emissions on tropospheric composition and radiation during 1997–2022. In the control simulation, fires emitted 530 ± 74 Tg CO yr^{-1}, accounting for 47 ± 3% of annual CO emissions from all sources. This contribution is larger than in many previous assessments, primarily because GFED5 includes substantially higher emissions from savanna, grassland, and agricultural fires as a result of improved burned-area mapping. Comparing simulations with and without fire emissions allowed us to isolate their effects on atmospheric chemistry, aerosols, and radiation over the 26-year study period. Fire emissions increased the global mean tropospheric CO column by 16 ± 2% and strongly influenced its seasonal and interannual variability, particularly over tropical continents and adjacent ocean regions. Their influence on the atmosphere's oxidative capacity was more complex. Fires increased OH by approximately 10–20% in the southern Amazon, central Africa, and tropical Asia, where emissions of NO_x and other reactive species interact with abundant sunlight and water vapor to promote OH formation. In contrast, fire-emitted CO consumes OH over broader and more remote regions, resulting in a net decrease in global mean tropospheric OH of approximately 4%. Fire emissions also increased the global mean tropospheric O_3 column by 6 ± 1%, with enhancements exceeding 20% over central Africa. Together, these results demonstrate that fires substantially alter tropospheric oxidation chemistry and that their effects on OH can differ in sign between source regions and the global atmosphere.

Fire emissions also substantially influenced atmospheric aerosols and radiation. They accounted for approximately 37% of global BC emissions, 73% of primary organic matter emissions, and 68% of secondary organic aerosol precursor emissions in the E3SM emissions framework. Consequently, fires increased global annual mean AOD by 7 ± 2% and substantially

https://doi.org/10.5194/egusphere-2026-4288
Preprint. Discussion started: 14 September 2026

improved the representation of seasonal and interannual AOD variability observed by MODIS in major tropical fire regions. Fire aerosols reduced surface shortwave radiation through direct and indirect effects, producing a net cooling influence. Fire-enhanced tropospheric O_3 produced shortwave and longwave warming that partially offset this aerosol cooling. Thus, the net radiative response to fire emissions emerges from interactions among chemically and radiatively active constituents with contrasting effects.

Our estimates are broadly consistent with previous modeling studies while highlighting the consequences of the larger fire emissions represented in GFED5. The approximately 4% reduction in global mean OH and +0.05 W m^{-2} O_3 radiative effect at the top of the atmosphere are similar to the 6% reduction and +0.03 W m^{-2} effect, respectively, simulated with GFDL-AM3 by Mao et al. (2013). In contrast, the 6 ± 1% fire contribution to the global tropospheric O_3 column is larger than the approximately 3.5% estimated by Jaffe and Wigder (2012). Similarly, the 47% contribution of fires to global CO emissions exceeds the approximately 40% reported in many previous studies. These differences are consistent with the higher savanna, grassland, and agricultural fire emissions in GFED5.

Model–observation comparisons provide additional evidence for the importance of these revised emissions, although they also reveal important regional biases. Including fires substantially improves the representation of the spatial distribution and seasonal and interannual variability of CO and AOD, particularly across tropical fire regions. For example, the model reproduces major CO and AOD anomalies associated with El Niño-related fire activity in tropical Asia and better represents the semiannual cycles of CO and AOD over central Africa. At the same time, positive O_3 biases over central Africa and remaining CO biases at northern high latitudes demonstrate that increasing fire emissions does not uniformly improve model performance. These contrasting

https://doi.org/10.5194/egusphere-2026-4288
Preprint. Discussion started: 14 September 2026

responses provide useful constraints on both the emissions inventory and atmospheric chemistry.

Relative to our earlier E3SMv1 analysis, which focused on aerosols without interactive atmospheric chemistry (Xu et al., 2021), the present E3SMv3 framework enables the effects of fires on OH, CO, and O_3 to be simulated together with aerosol and O_3 radiative effects. This coupled framework therefore provides a more complete representation of the chemical and radiative pathways through which fires influence atmospheric composition and climate. However, several uncertainties remain in both the fire emissions inventory and E3SM's representation of atmospheric processes. Fire emissions depend on uncertainties in burned area, fuel consumption, combustion completeness, land-cover classification, and emission factors. Although GFED5 improves the representation of burned area relative to earlier inventories, important uncertainties remain for small fires, peat combustion, and fuel consumption in boreal ecosystems. The high simulated CO and O_3 abundances over central Africa suggest that emissions from savanna fires may be overestimated or that their chemical speciation requires further refinement.

Other model–observation discrepancies point to uncertainties in atmospheric processing rather than fire emissions alone. The systematic negative AOD bias in E3SMv3 indicates a need to further evaluate aerosol production and removal processes, including wet and dry deposition. The fixed representation of fire injection heights also does not capture extreme pyrocumulonimbus events that transport smoke into the upper troposphere and lower stratosphere, increasing aerosol lifetimes and radiative impacts. Meanwhile, persistent CO underestimation at northern high latitudes likely reflects a combination of uncertainties in anthropogenic precursor emissions, atmospheric transport, and OH chemistry rather than a simple underestimate of boreal fire emissions. These regional model–observation mismatches provide useful constraints for improving future fire inventories and prognostic fire–chemistry models.

https://doi.org/10.5194/egusphere-2026-4288
Preprint. Discussion started: 14 September 2026

Taken together, our results demonstrate that fire emissions are an important component of the global atmospheric system, influencing air quality, oxidative capacity, aerosols, radiation, and climate from regional to global scales. Their atmospheric effects cannot be inferred from emissions alone because nonlinear chemistry and atmospheric processing determine both the magnitude and, in some cases, the sign of responses. This is particularly evident for OH, which increases in several major tropical fire regions but decreases globally, and for radiation, where aerosol cooling is partially offset by warming from fire-enhanced O_3. Accurately representing these coupled processes is therefore important for simulating contemporary atmospheric composition and for projecting how changes in fire regimes will influence climate and air quality. By combining paired fire and no-fire E3SMv3 simulations with satellite and surface observations, our analysis establishes diagnostics for evaluating the atmospheric consequences of fire emissions. Extending these diagnostics across additional observational datasets and applying them to prognostic fire simulations offers a pathway toward a systematic benchmark for evaluating coupled fire–chemistry–climate interactions in Earth system models.

Acknowledgements

This research was supported by the US Department of Energy's Biological and Environmental Research (BER) division in the Office of Science. This funding included support from the Earth System Model Development Program to the Energy Exascale Earth System Modeling Project. Additional support was provided by the Office of Science's Reducing Uncertainties in Biogeochemical Interactions through Synthesis and Computation Scientific Focus Area (RUBISCO SFA) in the Earth and Environmental Systems Modeling (EESM) Program under the Office of Biological and Environmental Research of the US Department of Energy Office of

https://doi.org/10.5194/egusphere-2026-4288
Preprint. Discussion started: 14 September 2026

Science. Qi Tang also acknowledges grant support from the US DOE CRC program via SCW1821 and Lawrence Livermore National Laboratory LDRD project 22-ERD-008. Part of this work was performed under the auspices of the U.S. DOE by Lawrence Livermore National Laboratory under Contract DE-AC52-07NA27344. Development of the GFED inventory was supported in part by NASA FireSense (80NSSC24K1317), FireTech (80NSSC24K1823), and CMS (80NSSC25K7211) grants to J. Randerson.

Code and Data Availability

Model code may be accessed at the GitHub repository https://github.com/E3SM-Project/E3SM. The fire emission data are publicly available from the Global Fire Emission Database version 5 (https://www.globalfiredata.org/). The level-3 monthly Terra-MODIS product (Collection 6.1) is publicly available at https://ladsweb.modaps.eosdis.nasa.gov/missions-and-measurements/products/MOD08_M3. The level 3 monthly MOPITT version 9 gridded data is available at https://terra.nasa.gov/about/terra-instruments/mopitt. The monthly gridded troposphere column ozone derived from the Aura Ozone Monitoring Instrument/Microwave Limb Sounder (OMI/MLS) is available at https://acd-ext.gsfc.nasa.gov/index.html. The monthly in-situ surface CO measurement are obtained from the Global Monitoring Laboratory (GML) of the National Oceanic and Atmospheric Administration (NOAA) (https://gml.noaa.gov/ccgg/data/co.html). The surface O_3 measurements are obtained from the Tropospheric Ozone Assessment Report (TOAR) database (https://toar-data.org/surface-data/). The E3SM simulations are available on request from the corresponding author.

Author Contributions

https://doi.org/10.5194/egusphere-2026-4288
Preprint. Discussion started: 14 September 2026

LX, QT, QZ, WJR and JTR designed the study. LX performed the model simulations and analyzed the model outputs. YC and GRvdW developed the GFED5 emission inventory. All authors contributed to data interpretation and the writing of the paper.

Competing Interests

The authors declare that they have no conflict of interest.

https://doi.org/10.5194/egusphere-2026-4288
Preprint. Discussion started: 14 September 2026

References

Akagi, S. K., Yokelson, R. J., Wiedinmyer, C., Alvarado, M. J., Reid, J. S., Karl, T., Crounse, J. D., and Wennberg, P. O.: Emission factors for open and domestic biomass burning for use in atmospheric models, Atmos Chem Phys, 11, 4039-4072, 10.5194/acp-11-4039-2011, 2011.

Alvarado, M. J., Logan, J. A., Mao, J., Apel, E., Riemer, D., Blake, D., Cohen, R. C., Min, K. E., Perring, A. E., Browne, E. C., Wooldridge, P. J., Diskin, G. S., Sachse, G. W., Fuelberg, H., Sessions, W. R., Harrigan, D. L., Huey, G., Liao, J., Case-Hanks, A., Jimenez, J. L., Cubison, M. J., Vay, S. A., Weinheimer, A. J., Knapp, D. J., Montzka, D. D., Flocke, F. M., Pollack, I. B., Wennberg, P. O., Kurten, A., Crounse, J., St Clair, J. M., Wisthaler, A., Mikoviny, T., Yantosca, R. M., Carouge, C. C., and Le Sager, P.: Nitrogen oxides and PAN in plumes from boreal fires during ARCTAS-B and their impact on ozone: an integrated analysis of aircraft and satellite observations, Atmos Chem Phys, 10, 9739-9760, 10.5194/acp-10-9739-2010, 2010.

Andela, N., Morton, D. C., Giglio, L., Chen, Y., van der Werf, G. R., Kasibhatla, P. S., DeFries, R. S., Collatz, G. J., Hantson, S., Kloster, S., Bachelet, D., Forrest, M., Lasslop, G., Li, F., Mangeon, S., Melton, J. R., Yue, C., and Randerson, J. T.: A human-driven decline in global burned area, Science, 356, 1356-1361, 10.1126/science.aal4108, 2017.

Andreae, M. O.: Emission of trace gases and aerosols from biomass burning - an updated assessment, Atmos Chem Phys, 19, 8523-8546, 10.5194/acp-19-8523-2019, 2019.

Archibald, A. T., O'Connor, F. M., Abraham, N. L., Archer-Nicholls, S., Chipperfield, M. P., Dalvi, M., Folberth, G. A., Dennison, F., Dhomse, S. S., Griffiths, P. T., Hardacre, C., Hewitt, A. J., Hill, R. S., Johnson, C. E., Keeble, J., Köhler, M. O., Morgenstern, O., Mulcahy, J. P., Ordóñez, C., Pope, R. J., Rumbold, S. T., Russo, M. R., Savage, N. H., Sellar, A., Stringer, M., Turnock, S. T., Wild, O., and Zeng, G.: Description and evaluation of the UKCA stratosphere-troposphere chemistry scheme (StratTrop vn 1.0) implemented in UKESM1, Geosci Model Dev, 13, 1223-1266, 10.5194/gmd-13-1223-2020, 2020.

Bellouin, N., Quaas, J., Gryspeerdt, E., Kinne, S., Stier, P., Watson-Parris, D., Boucher, O., Carslaw, K. S., Christensen, M., Daniau, A. L., Dufresne, J. L., Feingold, G., Fiedler, S., Forster, P., Gettelman, A., Haywood, J. M., Lohmann, U., Malavelle, F., Mauritsen, T., McCoy, D. T., Myhre, G., Mülmenstädt, J., Neubauer, D., Possner, A., Rugenstein, M., Sato, Y., Schulz, M., Schwartz, S. E., Sourdeval, O., Storelvmo, T., Toll, V., Winker, D., and Stevens, B.: Bounding Global Aerosol Radiative Forcing of Climate Change, Rev Geophys, 58, 10.1029/2019RG000660, 2020.

Bian, H., Chin, M., Kawa, S. R., Duncan, B., Arellano, A., and Kasibhatla, P.: Sensitivity of global CO simulations to uncertainties in biomass burning sources, J Geophys Res-Atmos, 112, 10.1029/2006jd008376, 2007.

https://doi.org/10.5194/egusphere-2026-4288
Preprint. Discussion started: 14 September 2026

712 Blanchard-Wrigglesworth, E., Derepentigny, P., and Frierson, D. M. W.: Increasing boreal fires
713 reduce future global warming and sea ice loss, P Natl Acad Sci USA, 122,
714 10.1073/pnas.2424614122, 2025.

715 Bond, T. C., Doherty, S. J., Fahey, D. W., Forster, P. M., Berntsen, T., DeAngelo, B. J., Flanner,
716 M. G., Ghan, S., Karcher, B., Koch, D., Kinne, S., Kondo, Y., Quinn, P. K., Sarofim, M.
717 C., Schultz, M. G., Schulz, M., Venkataraman, C., Zhang, H., Zhang, S., Bellouin, N.,
718 Guttikunda, S. K., Hopke, P. K., Jacobson, M. Z., Kaiser, J. W., Klimont, Z., Lohmann,
719 U., Schwarz, J. P., Shindell, D., Storelvmo, T., Warren, S. G., and Zender, C. S.:
720 Bounding the role of black carbon in the climate system: A scientific assessment, J
721 Geophys Res-Atmos, 118, 5380-5552, 10.1002/jgrd.50171, 2013.

722 Byrne, B., Liu, J. J., Bowman, K. W., Pascolini-Campbell, M., Chatterjee, A., Pandey, S.,
723 Miyazaki, K., van der Werf, G. R., Wunch, D., Wennberg, P. O., Roehl, C. M., and
724 Sinha, S.: Carbon emissions from the 2023 Canadian wildfires, Nature, 633,
725 10.1038/s41586-024-07878-z, 2024.

726 Chen, W., Zhang, Y. Z., Zou, Y. F., and Zhang, Z.: Climate feedback of forest fires amplified by
727 atmospheric chemistry, Nat Geosci, 19, 10.1038/s41561-026-01926-1, 2026.

728 Chen, Y., Morton, D. C., Andela, N., van der Werf, G. R., Giglio, L., and Randerson, J. T.: A
729 pan-tropical cascade of fire driven by El Nino/Southern Oscillation, Nat Clim Change, 7,
730 906-911, 10.1038/s41558-017-0014-8, 2017.

731 Chen, Y., Haywood, J., Wang, Y., Malavelle, F., Jordan, G., Partridge, D., Fieldsend, J., De
732 Leeuw, J., Schmidt, A., Cho, N., Oreopoulos, L., Platnick, S., Grosvenor, D., Field, P.,
733 and Lohmann, U.: Machine learning reveals climate forcing from aerosols is dominated
734 by increased cloud cover, Nat Geosci, 15, 609-614, 10.1038/s41561-022-00991-6, 2022.

735 Chen, Y., Hall, J., van Wees, D., Andela, N., Hantson, S., Giglio, L., van der Werf, G. R.,
736 Morton, D. C., and Randerson, J. T.: Multi-decadal trends and variability in burned area
737 from the fifth version of the Global Fire Emissions Database (GFED5), Earth Syst Sci
738 Data, 15, 5227-5259, 10.5194/essd-15-5227-2023, 2023.

739 Connolly, R., Marlier, M. E., Garcia-Gonzales, D. A., Wilkins, J., Su, J., Bekker, C., Jung, J.,
740 Bonilla, E., Burnett, R. T., Zhu, Y. F., and Jerrett, M.: Mortality attributable to PM2.5
741 from wildland fires in California from 2008 to 2018, Sci Adv, 10,
742 10.1126/sciadv.adl1252, 2024.

743 Coppola, A. I., Wagner, S., Lennartz, S. T., Seidel, M., Ward, N. D., Dittmar, T., Santín, C., and
744 Jones, M. W.: The black carbon cycle and its role in the Earth system, Nat Rev Earth
745 Env, 3, 516-532, 10.1038/s43017-022-00316-6, 2022.

746 Crutzen, P. J., and Andreae, M. O.: Biomass Burning in the Tropics - Impact on Atmospheric
747 Chemistry and Biogeochemical Cycles, Science, 250, 1669-1678,
748 10.1126/science.250.4988.1669, 1990.

https://doi.org/10.5194/egusphere-2026-4288
Preprint. Discussion started: 14 September 2026

Deeter, M. N., Mao, D., Martínez-Alonso, S., Worden, H. M., Andreae, M. O., and Schlager, H.: Impacts of MOPITT cloud detection revisions on observation frequency and mapping of highly polluted scenes, Remote Sens Environ, 262, 10.1016/j.rse.2021.112516, 2021.

Dennis, J. M., Edwards, J., Evans, K. J., Guba, O., Lauritzen, P. H., Mirin, A. A., St-Cyr, A., Taylor, M. A., and Worley, P. H.: CAM-SE: A scalable spectral element dynamical core for the Community Atmosphere Model, Int J High Perform C, 26, 74-89, 10.1177/1094342011428142, 2012.

Dlugokencky, E. J., Steele, L. P., Lang, P. M., and Masarie, K. A.: The Growth-Rate and Distribution of Atmospheric Methane, J Geophys Res-Atmos, 99, 17021-17043, 10.1029/94jd01245, 1994.

Emmons, L. K., Schwantes, R. H., Orlando, J. J., Tyndall, G., Kinnison, D., Lamarque, J. F., Marsh, D., Mills, M. J., Tilmes, S., Bardeen, C., Buchholz, R. R., Conley, A., Gettelman, A., Garcia, R., Simpson, I., Blake, D. R., Meinardi, S., and Petron, G.: The Chemistry Mechanism in the Community Earth System Model Version 2 (CESM2), J Adv Model Earth Sy, 12, 10.1029/2019MS001882, 2020.

Fasullo, J. T., Rosenbloom, N., and Buchholz, R.: A multiyear tropical Pacific cooling response to recent Australian wildfires in CESM2, Sci Adv, 9, 10.1126/sciadv.adg1213, 2023.

Feng, Y., Ramanathan, V., and Kotamarthi, V. R.: Brown carbon: a significant atmospheric absorber of solar radiation?, Atmos Chem Phys, 13, 8607-8621, 10.5194/acp-13-8607-2013, 2013.

Flanner, M. G., Zender, C. S., Randerson, J. T., and Rasch, P. J.: Present-day climate forcing and response from black carbon in snow, J Geophys Res-Atmos, 112, 10.1029/2006jd008003, 2007.

Gaubert, B., Arellano, A. F., Barré, J., Worden, H. M., Emmons, L. K., Tilmes, S., Buchholz, R. R., Vitt, F., Raeder, K., Collins, N., Anderson, J. L., Wiedinmyer, C., Alonso, S. M., Edwards, D. P., Andreae, M. O., Hannigan, J. W., Petri, C., Strong, K., and Jones, N.: Toward a chemical reanalysis in a coupled chemistry-climate model: An evaluation of MOPITT CO assimilation and its impact on tropospheric composition, J Geophys Res-Atmos, 121, 7310-7343, 10.1002/2016jd024863, 2016.

Gettelman, A., Mills, M. J., Kinnison, D. E., Garcia, R. R., Smith, A. K., Marsh, D. R., Tilmes, S., Vitt, F., Bardeen, C. G., McInerny, J., Liu, H. L., Solomon, S. C., Polvani, L. M., Emmons, L. K., Lamarque, J. F., Richter, J. H., Glanville, A. S., Bacmeister, J. T., Phillips, A. S., Neale, R. B., Simpson, I. R., DuVivier, A. K., Hodzic, A., and Randel, W. J.: The Whole Atmosphere Community Climate Model Version 6 (WACCM6), J Geophys Res-Atmos, 124, 12380-12403, 10.1029/2019jd030943, 2019.

Grieshop, A. P., Logue, J. M., Donahue, N. M., and Robinson, A. L.: Laboratory investigation of photochemical oxidation of organic aerosol from wood fires 1: measurement and simulation of organic aerosol evolution, Atmos Chem Phys, 9, 1263-1277, 10.5194/acp-9-1263-2009, 2009.

https://doi.org/10.5194/egusphere-2026-4288
Preprint. Discussion started: 14 September 2026

788 Hatch, L. E., Yokelson, R. J., Stockwell, C. E., Veres, P. R., Simpson, I. J., Blake, D. R.,
789 Orlando, J. J., and Barsanti, K. C.: Multi-instrument comparison and compilation of non-
790 methane organic gas emissions from biomass burning and implications for smoke-derived
791 secondary organic aerosol precursors, Atmos Chem Phys, 17, 1471-1489, 10.5194/acp-
792 17-1471-2017, 2017.

793 Hodzic, A., Jimenez, J. L., Madronich, S., Canagaratna, M. R., DeCarlo, P. F., Kleinman, L., and
794 Fast, J.: Modeling organic aerosols in a megacity: potential contribution of semi-volatile
795 and intermediate volatility primary organic compounds to secondary organic aerosol
796 formation, Atmos Chem Phys, 10, 5491-5514, 10.5194/acp-10-5491-2010, 2010.

797 Hoesly, R. M., Smith, S. J., Feng, L. Y., Klimont, Z., Janssens-Maenhout, G., Pitkanen, T.,
798 Seibert, J. J., Vu, L., Andres, R. J., Bolt, R. M., Bond, T. C., Dawidowski, L., Kholod, N.,
799 Kurokawa, J., Li, M., Liu, L., Lu, Z. F., Moura, M. C. P., O'Rourke, P. R., and Zhang, Q.:
800 Historical (1750-2014) anthropogenic emissions of reactive gases and aerosols from the
801 Community Emissions Data System (CEDS), Geosci Model Dev, 11, 369-408,
802 10.5194/gmd-11-369-2018, 2018.

803 Hooghiemstra, P. B., Krol, M. C., Bergamaschi, P., de Laat, A. T. J., van der Werf, G. R.,
804 Novelli, P. C., Deeter, M. N., Aben, I., and Röckmann, T.: Comparing optimized CO
805 emission estimates using MOPITT or NOAA surface network observations, J Geophys
806 Res-Atmos, 117, 10.1029/2011jd017043, 2012.

807 Horowitz, L. W., Naik, V., Paulot, F., Ginoux, P. A., Dunne, J. P., Mao, J. Q., Schnell, J., Chen,
808 X., He, J., John, J. G., Lin, M. Y., Lin, P., Malyshev, S., Paynter, D., Shevliakova, E., and
809 Zhao, M.: The GFDL Global Atmospheric Chemistry-Climate Model AM4.1: Model
810 Description and Simulation Characteristics, J Adv Model Earth Sy, 12,
811 10.1029/2019MS002032, 2020.

812 Hsu, J., and Prather, M. J.: Global long-lived chemical modes excited in a 3-D chemistry
813 transport model: Stratospheric N_2O, NO_y, O_3 and CH_4 chemistry, Geophys Res Lett, 37,
814 L07805, 10.1029/2009gl042243, 2010.

815 Hu, A. L., Ke, Z. M., Liu, X. H., Wagman, B., Brown, H., Lu, Z., Wu, M. X., Wang, H. L.,
816 Tang, Q., Bull, D., Peterson, K., and Xie, S. C.: Size-resolved process understanding of
817 stratospheric sulfate aerosol following the Pinatubo eruption, Atmos Chem Phys, 25,
818 12137-12157, 10.5194/acp-25-12137-2025, 2025.

819 Hurrell, J. W., Hack, J. J., Shea, D., Caron, J. M., and Rosinski, J.: A new sea surface
820 temperature and sea ice boundary dataset for the Community Atmosphere Model, J
821 Climate, 21, 5145-5153, 10.1175/2008jcli2292.1, 2008.

822 Jaffe, D. A., and Wigder, N. L.: Ozone production from wildfires: A critical review, Atmos
823 Environ, 51, 1-10, 10.1016/j.atmosenv.2011.11.063, 2012.

824 Jathar, S. H., Farina, S. C., Robinson, A. L., and Adams, P. J.: The influence of semi-volatile and
825 reactive primary emissions on the abundance and properties of global organic aerosol,
826 Atmos Chem Phys, 11, 7727-7746, 10.5194/acp-11-7727-2011, 2011.

https://doi.org/10.5194/egusphere-2026-4288
Preprint. Discussion started: 14 September 2026

Jimenez, J. L., Canagaratna, M. R., Donahue, N. M., Prevot, A. S. H., Zhang, Q., Kroll, J. H., DeCarlo, P. F., Allan, J. D., Coe, H., Ng, N. L., Aiken, A. C., Docherty, K. S., Ulbrich, I. M., Grieshop, A. P., Robinson, A. L., Duplissy, J., Smith, J. D., Wilson, K. R., Lanz, V. A., Hueglin, C., Sun, Y. L., Tian, J., Laaksonen, A., Raatikainen, T., Rautiainen, J., Vaattovaara, P., Ehn, M., Kulmala, M., Tomlinson, J. M., Collins, D. R., Cubison, M. J., Dunlea, E. J., Huffman, J. A., Onasch, T. B., Alfarra, M. R., Williams, P. I., Bower, K., Kondo, Y., Schneider, J., Drewnick, F., Borrmann, S., Weimer, S., Demerjian, K., Salcedo, D., Cottrell, L., Griffin, R., Takami, A., Miyoshi, T., Hatakeyama, S., Shimono, A., Sun, J. Y., Zhang, Y. M., Dzepina, K., Kimmel, J. R., Sueper, D., Jayne, J. T., Herndon, S. C., Trimborn, A. M., Williams, L. R., Wood, E. C., Middlebrook, A. M., Kolb, C. E., Baltensperger, U., and Worsnop, D. R.: Evolution of Organic Aerosols in the Atmosphere, Science, 326, 1525-1529, 10.1126/science.1180353, 2009.

Jin, X. M., Zhu, Q. D., and Cohen, R. C.: Direct estimates of biomass burning NO_x emissions and lifetimes using daily observations from TROPOMI, Atmos Chem Phys, 21, 15569-15587, 10.5194/acp-21-15569-2021, 2021.

Johnston, F. H., Henderson, S. B., Chen, Y., Randerson, J. T., Marlier, M., DeFries, R. S., Kinney, P., Bowman, D. M. J. S., and Brauer, M.: Estimated Global Mortality Attributable to Smoke from Landscape Fires, Environ Health Persp, 120, 695-701, 10.1289/ehp.1104422, 2012.

Johnston, F. H., Borchers-Arriagada, N., Morgan, G. G., Jalaludin, B., Palmer, A. J., Williamson, G. J., and Bowman, D. M. J.: Unprecedented health costs of smoke-related PM2.5 from the 2019–20 Australian megafires, Nat Sustain, 4, 42–47, 10.1038/s41893-020-00610-5, 2021.

Kang, S. C., Zhang, Y. L., Qian, Y., and Wang, H. L.: A review of black carbon in snow and ice and its impact on the cryosphere, Earth-Sci Rev, 210, 10.1016/j.earscirev.2020.103346, 2020.

Ke, Z. M., Tang, Q., Zhang, J. S., Chen, Y., Randerson, J., Li, J. F., and Zhang, Y. Y.: Simulating Pyrocumulonimbus Clouds Using a Multiscale Wildfire Simulation Framework, Geophys Res Lett, 52, 10.1029/2024GL114025, 2025.

Kelesidis, G. A., Moularas, C., Parhizkar, H., Calderon, L., Tsiodra, I., Mihalopoulos, N., Kavouras, I., Korras-Carraca, M. B., Hatzianastassiou, N., Georgopoulos, P. G., Laurent, J. G. C., and Demokritou, P.: Radiative cooling in New York/New Jersey metropolitan areas by wildfire particulate matter emitted from the Canadian wildfires of 2023, Commun Earth Environ, 6, 10.1038/s43247-025-02214-3, 2025.

Koo, B., Knipping, E., and Yarwood, G.: 1.5-Dimensional volatility basis set approach for modeling organic aerosol in CAMx and CMAQ, Atmos Environ, 95, 158-164, 10.1016/j.atmosenv.2014.06.031, 2014.

Liu, J. J., Bowman, K. W., Schimel, D. S., Parazoo, N. C., Jiang, Z., Lee, M., Bloom, A. A., Wunch, D., Frankenberg, C., Sun, Y., O'Dell, C. W., Gurney, K. R., Menemenlis, D., Gierach, M., Crisp, D., and Eldering, A.: Contrasting carbon cycle responses of the

https://doi.org/10.5194/egusphere-2026-4288
Preprint. Discussion started: 14 September 2026

tropical continents to the 2015-2016 El Niño, Science, 358, 10.1126/science.aam5690, 2017.

Liu, X., Easter, R. C., Ghan, S. J., Zaveri, R., Rasch, P., Shi, X., Lamarque, J. F., Gettelman, A., Morrison, H., Vitt, F., Conley, A., Park, S., Neale, R., Hannay, C., Ekman, A. M. L., Hess, P., Mahowald, N., Collins, W., Iacono, M. J., Bretherton, C. S., Flanner, M. G., and Mitchell, D.: Toward a minimal representation of aerosols in climate models: description and evaluation in the Community Atmosphere Model CAM5, Geosci Model Dev, 5, 709-739, 10.5194/gmd-5-709-2012, 2012.

Lombardozzi, D., Sparks, J. P., and Bonan, G.: Integrating O-3 influences on terrestrial processes: photosynthetic and stomatal response data available for regional and global modeling, Biogeosciences, 10, 6815-6831, 10.5194/bg-10-6815-2013, 2013.

Lou, S. J., Shrivastava, M., Easter, R. C., Yang, Y., Ma, P. L., Wang, H. L., Cubison, M. J., Campuzano-Jost, P., Jimenez, J. L., Zhang, Q., Rasch, P. J., Shilling, J. E., Zelenyuk, A., Dubey, M., Cameron-Smith, P., Martin, S. T., Schneider, J., and Schulz, C.: New SOA Treatments Within the Energy Exascale Earth System Model (E3SM): Strong Production and Sinks Govern Atmospheric SOA Distributions and Radiative Forcing, J Adv Model Earth Sy, 12, e2020MS002266, 10.1029/2020MS002266, 2020.

Mao, J. Q., Horowitz, L. W., Naik, V., Fan, S. M., Liu, J. F., and Fiore, A. M.: Sensitivity of tropospheric oxidants to biomass burning emissions: implications for radiative forcing, Geophys Res Lett, 40, 1241-1246, 10.1002/grl.50210, 2013.

Oliveira, P. H. F., Artaxo, P., Pires, C., De Lucca, S., Procopio, A., Holben, B., Schafer, J., Cardoso, L. F., Wofsy, S. C., and Rocha, H. R.: The effects of biomass burning aerosols and clouds on the CO2 flux in Amazonia, Tellus B, 59, 338-349, 10.1111/j.1600-0889.2007.00270.x, 2007.

Olivier, J. G. J., Van Aardenne, J. A., Dentener, F. J., Pagliari, V., Ganzeveld, L. N., and Peters, J. A. H. W.: Recent trends in global greenhouse gas emissions:regional trends 1970–2000 and spatial distributionof key sources in 2000, Environmental Sciences, 2, 81-99, 10.1080/15693430500400345, 2005.

Palm, B. B., Peng, Q. Y., Fredrickson, C. D., Lee, B., Garofalo, L. A., Pothier, M. A., Kreidenweis, S. M., Farmer, D. K., Pokhrel, R. P., Shen, Y. J., Murphy, S. M., Permar, W., Hu, L., Campos, T. L., Hall, S. R., Ullmann, K., Zhang, X., Flocke, F., Fischer, E., and Thornton, J. A.: Quantification of organic aerosol and brown carbon evolution in fresh wildfire plumes, P Natl Acad Sci USA, 117, 29469-29477, 10.1073/pnas.2012218117, 2020.

Penner, J. E., Dickinson, R. E., and O'neill, C. A.: Effects of Aerosol from Biomass Burning on the Global Radiation Budget, Science, 256, 1432-1434, 10.1126/science.256.5062.1432, 1992.

Penner, J. E., Chuang, C. C., and Grant, K.: Climate forcing by carbonaceous and sulfate aerosols, Clim Dynam, 14, 839-851, 10.1007/s003820050259, 1998.

https://doi.org/10.5194/egusphere-2026-4288
Preprint. Discussion started: 14 September 2026

Peterson, D. A., Fromm, M. D., McRae, R. H. D., Campbell, J. R., Hyer, E. J., Taha, G., Camacho, C. P., Kablick, G., Schmidt, C. C., and DeLand, M. T.: Australia's Black Summer pyrocumulonimbus super outbreak reveals potential for increasingly extreme stratospheric smoke events, Npj Clim Atmos Sci, 4, 38, 10.1038/s41612-021-00192-9, 2021.

Prather, M. J., Holmes, C. D., and Hsu, J.: Reactive greenhouse gas scenarios: Systematic exploration of uncertainties and the role of atmospheric chemistry, Geophys Res Lett, 39, L09803, 10.1029/2012gl051440, 2012.

Prather, M. J., and Zhu, L.: Resetting tropospheric OH and CH4 lifetime with ultraviolet H2O absorption, Science, 385, 201-204, 10.1126/science.adn0415, 2024a.

Prather, M. J., and Zhu, X.: Lifetimes and timescales of tropospheric ozone, Elementa-Sci Anthrop, 12 (1), 10.1525/elementa.2023.00112, 2024b.

Prather, M. J.: Calibrating the Tropospheric Air and Ozone Mass, Agu Adv, 6, 10.1029/2025AV001651, 2025.

Ramanathan, V., Callis, L., Cess, R., Hansen, J., Isaksen, I., Kuhn, W., Lacis, A., Luther, F., Mahlman, J., Reck, R., and Schlesinger, M.: Climate-Chemical Interactions and Effects of Changing Atmospheric Trace Gases, Rev Geophys, 25, 1441-1482, 10.1029/RG025i007p01441, 1987.

Ramanathan, V., and Carmichael, G.: Global and regional climate changes due to black carbon, Nat Geosci, 1, 221-227, 10.1038/ngeo156, 2008.

Réveillet, M., Dumont, M., Gascoin, S., Lafaysse, M., Nabat, P., Ribes, A., Nheili, R., Tuzet, F., Ménégoz, M., Morin, S., Picard, G., and Ginoux, P.: Black carbon and dust alter the response of mountain snow cover under climate change, Nat Commun, 13, 10.1038/s41467-022-32501-y, 2022.

Robinson, A. L., Donahue, N. M., Shrivastava, M. K., Weitkamp, E. A., Sage, A. M., Grieshop, A. P., Lane, T. E., Pierce, J. R., and Pandis, S. N.: Rethinking organic aerosols: Semivolatile emissions and photochemical aging, Science, 315, 1259-1262, 10.1126/science.1133061, 2007.

Sayer, A. M., Munchak, L. A., Hsu, N. C., Levy, R. C., Bettenhausen, C., and Jeong, M. J.: MODIS Collection 6 aerosol products: Comparison between Aqua's e-Deep Blue, Dark Target, and "merged" data sets, and usage recommendations, J Geophys Res-Atmos, 119, 13965-13989, 10.1002/2014jd022453, 2014.

Shahid, S. B., Lacey, F. G., Wiedinmyer, C., Yokelson, R. J., and Barsanti, K. C.: NEIVAv1.0: Next-generation Emissions InVentory expansion of Akagi et al. (2011) version 1.0, Geosci Model Dev, 17, 7679-7711, 10.5194/gmd-17-7679-2024, 2024.

Shrivastava, M., Easter, R. C., Liu, X. H., Zelenyuk, A., Singh, B., Zhang, K., Ma, P. L., Chand, D., Ghan, S., Jimenez, J. L., Zhang, Q., Fast, J., Rasch, P. J., and Tiitta, P.: Global

https://doi.org/10.5194/egusphere-2026-4288
Preprint. Discussion started: 14 September 2026

transformation and fate of SOA: Implications of low-volatility SOA and gas-phase fragmentation reactions, J Geophys Res-Atmos, 120, 4169-4195, 10.1002/2014jd022563, 2015.

Sindelarova, K., Granier, C., Bouarar, I., Guenther, A., Tilmes, S., Stavrakou, T., Müller, J. F., Kuhn, U., Stefani, P., and Knorr, W.: Global data set of biogenic VOC emissions calculated by the MEGAN model over the last 30 years, Atmos Chem Phys, 14, 9317-9341, 10.5194/acp-14-9317-2014, 2014.

Skiles, S. M., Flanner, M., Cook, J. M., Dumont, M., and Painter, T. H.: Radiative forcing by light-absorbing particles in snow, Nat Clim Change, 8, 964-971, 10.1038/s41558-018-0296-5, 2018.

Szopa, S., Naik, V., Adhikary, B., Artaxo, P., Berntsen, T., Collins, W. D., Fuzzi, S., Gallardo, L., Kiendler-Scharr, A., Klimont, Z., Liao, H., Unger, N., and Zanis, P.: Short-lived Climate Forcers, in: Climate Change 2021 – The Physical Science Basis: Working Group I Contribution to the Sixth Assessment Report of the Intergovernmental Panel on Climate Change, edited by: Intergovernmental Panel on Climate, C., Cambridge University Press, Cambridge, 817-922, 2021.

Tang, Q., Prather, M. J., Ke, Z. M., Xie, J. B., Lee, H.-H., Wu, M. X., Cameron-Smith, P., Wang, H. L., Lin, W. Y., and Xie, S. C.: Interactive Gas Chemistry for Enhanced Science Capabilities of the Energy Exascale Earth System Model Version 3, J Adv Model Earth Sy, 17, e2025MS005062, 10.1029/2025MS005062, 2025.

Taylor, M. A., and Fournier, A.: A compatible and conservative spectral element method on unstructured grids, J Comput Phys, 229, 5879-5895, 10.1016/j.jcp.2010.04.008, 2010.

Thornhill, G. D., Collins, W. J., Kramer, R. J., Olivi, D., Skeie, R. B., O'Connor, F. M., Abraham, N. L., Checa-Garcia, R., Bauer, S. E., Deushi, M., Emmons, L. K., Forster, P. M., Horowitz, L. W., Johnson, B., Keeble, J., Lamarque, J. F., Michou, M., Mills, M. J., Mulcahy, J. P., Myhre, G., Nabat, P., Naik, V., Oshima, N., Schulz, M., Smith, C. J., Takemura, T., Tilmes, S., Wu, T. W., Zeng, G., and Zhang, J.: Effective radiative forcing from emissions of reactive gases and aerosols - a multi-model comparison, Atmos Chem Phys, 21, 853-874, 10.5194/acp-21-853-2021, 2021.

Tsimpidi, A. P., Karydis, V. A., Zavala, M., Lei, W., Molina, L., Ulbrich, I. M., Jimenez, J. L., and Pandis, S. N.: Evaluation of the volatility basis-set approach for the simulation of organic aerosol formation in the Mexico City metropolitan area, Atmos Chem Phys, 10, 525-546, 10.5194/acp-10-525-2010, 2010.

val Martin, M., Kahn, R. A., and Tosca, M. G.: A Global Analysis of Wildfire Smoke Injection Heights Derived from Space-Based Multi-Angle Imaging, Remote Sens-Basel, 10, 10.3390/rs10101609, 2018.

van der Velde, I. R., van der Werf, G. R., Houweling, S., Maasakkers, J. D., Borsdorff, T., Landgraf, J., Tol, P., van Kempen, T. A., van Hees, R., Hoogeveen, R., Veefkind, J. P.,

https://doi.org/10.5194/egusphere-2026-4288
Preprint. Discussion started: 14 September 2026

and Aben, I.: Vast CO_2 release from Australian fires in 2019-2020 constrained by satellite, Nature, 597, 366–369, 10.1038/s41586-021-03712-y, 2021.

van der Werf, G. R., Randerson, J. T., Collatz, G. J., Giglio, L., Kasibhatla, P. S., Arellano, A. J. r., Olsen, S. C., and Kasischke, E. S.: Continental-scale partitioning of fire emissions during the 1997 to 2001 El Nino/La Nina period, Science, 303, 73-76, 10.1126/science.1090753, 2004.

van der Werf, G. R., Randerson, J. T., van Wees, D., Chen, Y., Giglio, L., Hall, J., Roland, V., Mu, M. Q., Shahid, S. B., Barsanti, K. C., Yokelson, R., and Morton, D. C.: Landscape fire emissions from the 5th version of the Global Fire Emissions Database (GFED5), Sci Data, 12, 10.1038/s41597-025-06127-w, 2025.

van Gerrevink, M. J., Veraverbeke, S., Cooperdock, S., Potter, S., Zhong, Q. R., Moubarak, M., Virkkala, A. M., Goetz, S. J., Mack, M. C., Randerson, J. T., Schutgens, N., Turetsky, M. R., van der Werf, G. R., and Rogers, B. M.: Climate impacts from North American boreal forest fires, Nat Geosci, 19, 10.1038/s41561-026-01940-3, 2026.

van Leeuwen, T. T., Peters, W., Krol, M. C., and van der Werf, G. R.: Dynamic biomass burning emission factors and their impact on atmospheric CO mixing ratios, J Geophys Res-Atmos, 118, 6797-6815, 10.1002/jgrd.50478, 2013.

Wiedinmyer, C., Akagi, S. K., Yokelson, R. J., Emmons, L. K., Al-Saadi, J. A., Orlando, J. J., and Soja, A. J.: The Fire INventory from NCAR (FINN): a high resolution global model to estimate the emissions from open burning, Geosci Model Dev, 4, 625-641, 10.5194/gmd-4-625-2011, 2011.

Xie, S. C., Terai, C. R., Wang, H. L., Tang, Q., Fan, J. W., Burrows, S., Lin, W. Y., Wu, M. X., Song, X. L., Zhang, Y. Y., Taylor, M. A., Golaz, J., Benedict, J. J., Chen, C. H. H., Feng, Y., Hannah, W. M., Ke, Z. M., Shan, Y. P., Larson, V. E., Liu, X. H., Prather, M. J., Richter, J. H., Shrivastava, M., Wan, H., Zhang, G. J., Zhang, K., Bradley, A. M., Cameron-Smith, P., Damiano, L., Debusschere, B. J., Donahue, A. S., Easter, R. C., Eldred, M. S., Griffin, B. M., Guba, O., Guo, Z., Huang, X. L., Lee, J. W., Lee, H.-H., Lou, S. J., Mahfouz, N., Moncrieff, M., Mülmenstädt, J., Qian, Y., Rasool, Q. Z., Roberts, A. F., Santos, S. P., Sargsyan, K., Shpund, J., Singh, B., Tao, C., Xie, J. B., Yang, Y., Zeng, X. B., Zhang, C. Z., Zhang, M., Zhang, S. X., Zhang, T., Zheng, X., Jacob, R. L., Leung, L. R., McCoy, R. B., and Bader, D. C.: The Energy Exascale Earth System Model Version 3: 1. Overview of the Atmospheric Component, J Adv Model Earth Sy, 17, 10.1029/2025MS005120, 2025.

Xie, Y. Y., Lin, M. Y., Decharme, B., Delire, C., Horowitz, L. W., Lawrence, D. M., Li, F., and Séférian, R.: Tripling of western US particulate pollution from wildfires in a warming climate, P Natl Acad Sci USA, 119, 10.1073/pnas.2111372119, 2022.

Xu, L., Zhu, Q., Riley, W. J., Chen, Y., Wang, H. L., Ma, P. L., and Randerson, J. T.: The Influence of Fire Aerosols on Surface Climate and Gross Primary Production in the Energy Exascale Earth System Model (E3SM), J Climate, 34, 7219-7238, 10.1175/Jcli-D-21-0193.1, 2021.

https://doi.org/10.5194/egusphere-2026-4288
Preprint. Discussion started: 14 September 2026

Xu, L. L., Lin, G. X., Wu, C. L., Chen, X., Wang, H., Chen, C., Chakrabarty, R. K., Gao, M., Vakkari, V., van Zyl, P. G., and Liu, X. H.: Strong global radiative effects from wildfire dark brown carbon, Nat Geosci, 19, 10.1038/s41561-026-01972-9, 2026.

Zhang, D. L., Wang, W. H., Xi, Y. Z., Bi, J. Z., Hang, Y., Zhu, Q. Y., Pu, Q., Chang, H., and Liu, Y.: Wildland Fires Worsened Population Exposure to PM2.5 Pollution in the Contiguous United States, Environ Sci Technol, 57, 19990-19998, 10.1021/acs.est.3c05143, 2023.

Zhang, Q., Wang, Y. X. Z., Xiao, Q. Y., Geng, G. N., Davis, S. J., Liu, X. D., Yang, J., Liu, J. J., Huang, W. Y., He, C. P., Luo, B. H., Martin, R. V., Brauer, M., Randerson, J. T., and He, K. B.: Long-range PM2.5 pollution and health impacts from the 2023 Canadian wildfires, Nature, 645, 10.1038/s41586-025-09482-1, 2025.

Zhao, Y. H., Saunois, M., Bousquet, P., Lin, X., Berchet, A., Hegglin, M. I., Canadell, J. G., Jackson, R. B., Hauglustaine, D. A., Szopa, S., Stavert, A. R., Abraham, N. L., Archibald, A. T., Bekki, S., Deushi, M., Jöckel, P., Josse, B., Kinnison, D., Kirner, O., Marécal, V., O'Connor, F. M., Plummer, D. A., Revell, L. E., Rozanov, E., Stenke, A., Strode, S., Tilmes, S., Dlugokencky, E. J., and Zheng, B.: Inter-model comparison of global hydroxyl radical (OH) distributions and their impact on atmospheric methane over the 2000-2016 period, Atmos Chem Phys, 19, 13701-13723, 10.5194/acp-19-13701-2019, 2019.

Zheng, B., Chevallier, F., Yin, Y., Ciais, P., Fortems-Cheiney, A., Deeter, M. N., Parker, R. J., Wang, Y. L., Worden, H. M., and Zhao, Y. H.: Global atmospheric carbon monoxide budget 2000-2017 inferred from multi-species atmospheric inversions, Earth Syst Sci Data, 11, 1411-1436, 10.5194/essd-11-1411-2019, 2019.

Zheng, B., Ciais, P., Chevallier, F., Yang, H., Canadell, J. G., Chen, Y., van der Velde, I. R., Aben, I., Chuvieco, E., Davis, S. J., Deeter, M., Hong, C. P., Kong, Y. W., Li, H. Y., Li, H., Lin, X., He, K. B., and Zhang, Q.: Record-high CO_2 emissions from boreal fires in 2021, Science, 379, 912-917, 10.1126/science.ade0805, 2023.

Zhu, J. L., Penner, J. E., Lin, G. X., Zhou, C., Xu, L., and Zhuang, B. L.: Mechanism of SOA formation determines magnitude of radiative effects, P Natl Acad Sci USA, 114, 12685-12690, 10.1073/pnas.1712273114, 2017.

Ziemke, J. R., Chandra, S., Duncan, B. N., Froidevaux, L., Bhartia, P. K., Levelt, P. F., and Waters, J. W.: Tropospheric ozone determined from aura OMI and MLS: Evaluation of measurements and comparison with the Global Modeling Initiative's Chemical Transport Model, J Geophys Res-Atmos, 111, D19303, 10.1029/2006jd007089, 2006.

https://doi.org/10.5194/egusphere-2026-4288
Preprint. Discussion started: 14 September 2026

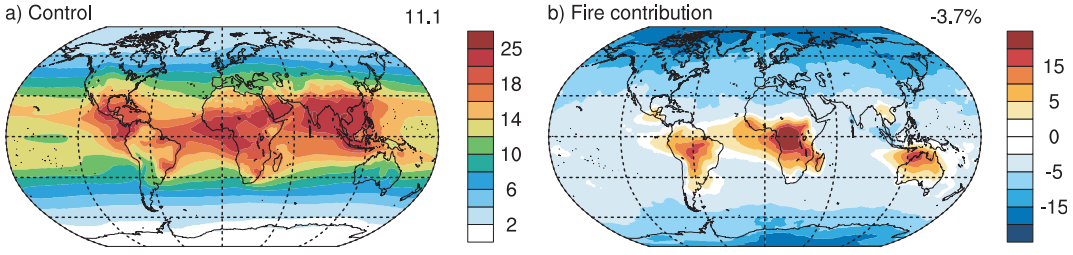

Figure 1: Annual average tropospheric OH concentration (unit: 10^5 molecules cm^{-3}) during 1997-2022 for a) the control run, and b) fire contribution (unit: %) computed as the absolute difference between the control and no-fire simulations relative to the control simulation. The tropospheric average OH concentration is calculated from the surface to 200 hPa. The global area-weighted mean values are given in the upper right corner of each panel.

https://doi.org/10.5194/egusphere-2026-4288
Preprint. Discussion started: 14 September 2026

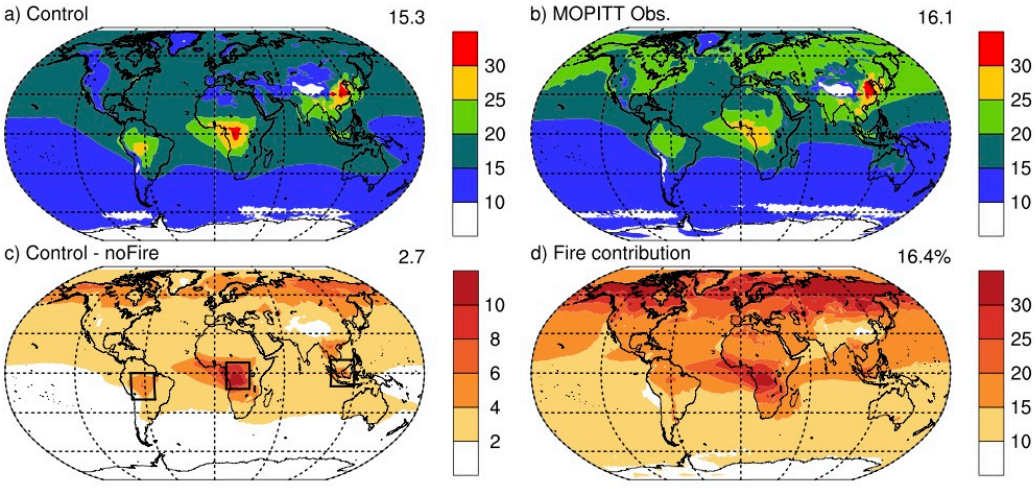

Figure 2: Annual average CO column (unit: 10^{17} molecules cm^{-2}) during 2000-2022 for a) the control run, b) the MOPITT satellite observations, c) the difference (10^{17} molecules cm^{-2}) between the control and no-fire runs and d) the fire contribution (unit: %) computed as the difference between the control and no-fire simulations relative to the control simulation. The global area weighted mean values are displayed in the upper right corner of each panel. The three selected 20°×20° tropical regions in the southern Amazon, central Africa, and tropical Asia that characterized by strong fire influence are marked with black squares in Figure 2c. We report time series from these regions in subsequent analyses.

https://doi.org/10.5194/egusphere-2026-4288
Preprint. Discussion started: 14 September 2026

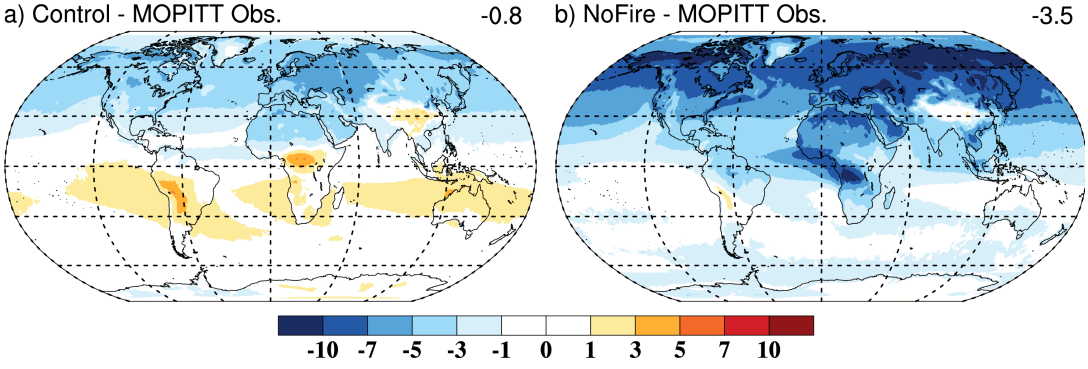

Figure 3: Mean annual average CO column differences (unit: 10^{17} molecules cm^{-2}) during 2000-2022 between MOPITT satellite observations and a) the control run and b) the no-fire run. The global area-weighted mean values are shown in upper right corner of each panel.

https://doi.org/10.5194/egusphere-2026-4288
Preprint. Discussion started: 14 September 2026

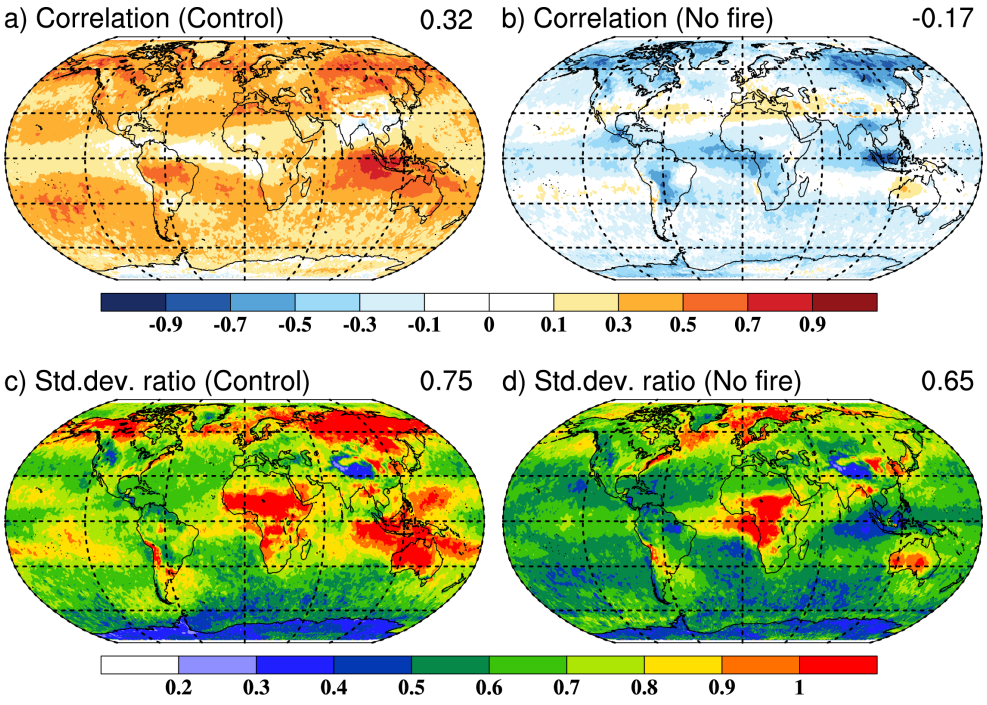

Figure 4: The correlation and ratio of standard deviations between E3SM simulations and MOPITT column CO observations for CO anomalies. The first row shows the correlation between monthly column CO anomalies from the control simulation, including fire emissions, and the observation in panel a), and the same for the no-fire simulation in panel b). The anomalies were computed by removing a mean annual cycle of column CO from the original data at each grid cell separately for the model and MOPITT satellite observations. The second row shows the ratio of the standard deviations of the anomalies for the model simulation and the MOPITT observations for the control simulation (panel c) and the no-fire simulation (panel d). The global area-weighted mean values are shown in the upper right corner of each panel.

https://doi.org/10.5194/egusphere-2026-4288
Preprint. Discussion started: 14 September 2026

1125
1126
1127

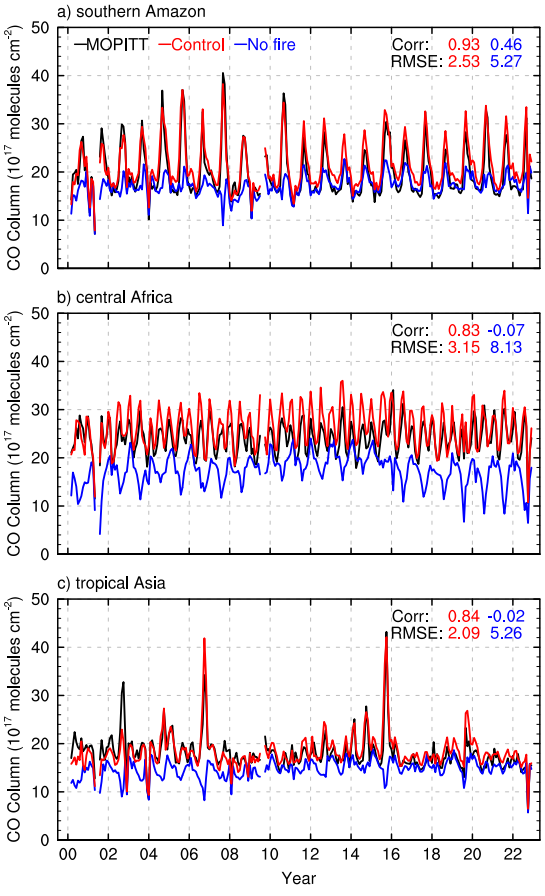

Figure 5: Time series of the MOPITT observed and modeled CO column (10^{17} molecules cm^{-2}) from the control (red line) and no-fire (blue line) simulations during 2000-2022 in a) southern Amazon, b) central Africa, and c) tropical Asia. The Pearson correlation and root mean square error (i.e., RMSE) between the modeled and observed values are given in each panel. The red and blue values represent the computed values for the control and no-fire simulations, respectively.

https://doi.org/10.5194/egusphere-2026-4288
Preprint. Discussion started: 14 September 2026

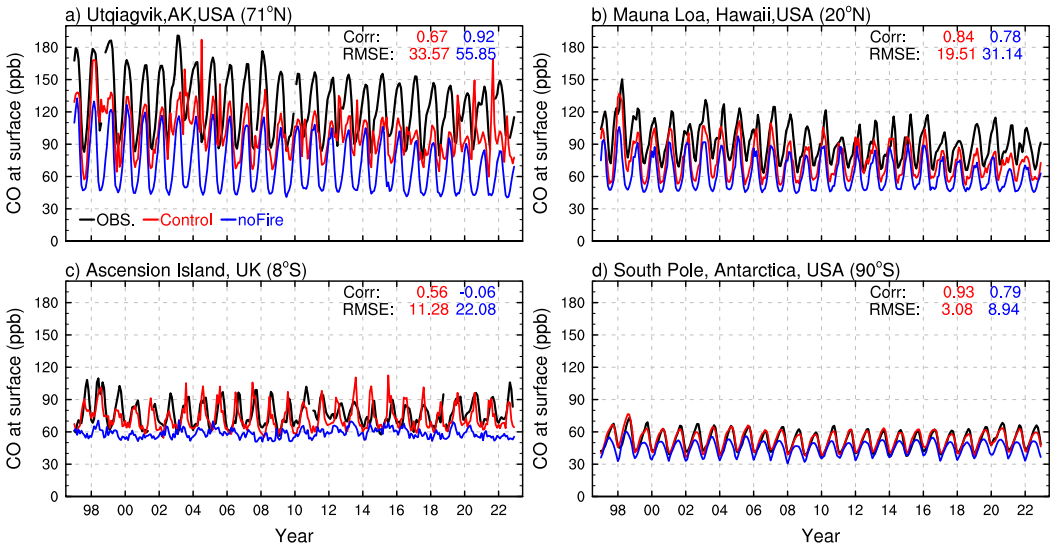

Figure 6: Surface CO mixing ratio (ppb) derived during 1997-2022 for the control run, no-fire run and observations in a) Utqiaġvik, AK, USA (formerly Point Barrow), b) Mauna Loa, USA, c) Ascension Island, UK, and d) South Pole, Antarctica, USA. The Pearson correlation and root mean square error (i.e., RMSE) between the modeled and observed values are given in each panel. The red and blue values represent the computed values for the control and no-fire simulations, respectively.

https://doi.org/10.5194/egusphere-2026-4288
Preprint. Discussion started: 14 September 2026

1147
1148
1149

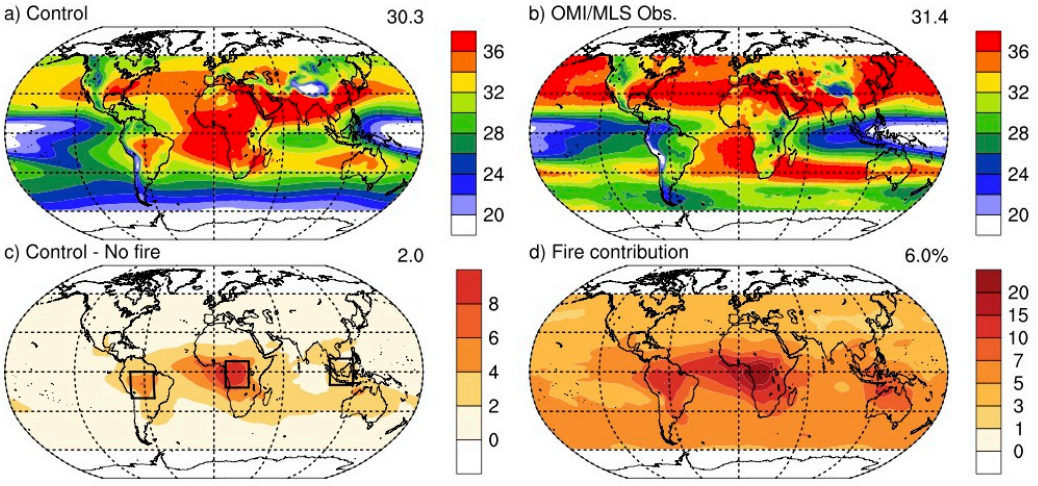

Figure 7: Annual average tropospheric column O_3 (DU) for a) the control run, b) the OMI/MLS satellite climatology observations during 2005-2020, c) the difference (DU) between the control and no-fire runs, and d) fire contribution in terms of the relative percentage difference (%) between the control and no-fire runs. The selected 20°×20° three tropical regions in Southern Amazon, Central Africa and Tropical Asia are marked with black squares. The global area-weighted mean values are shown in the upper right corner of each panel.

https://doi.org/10.5194/egusphere-2026-4288
Preprint. Discussion started: 14 September 2026

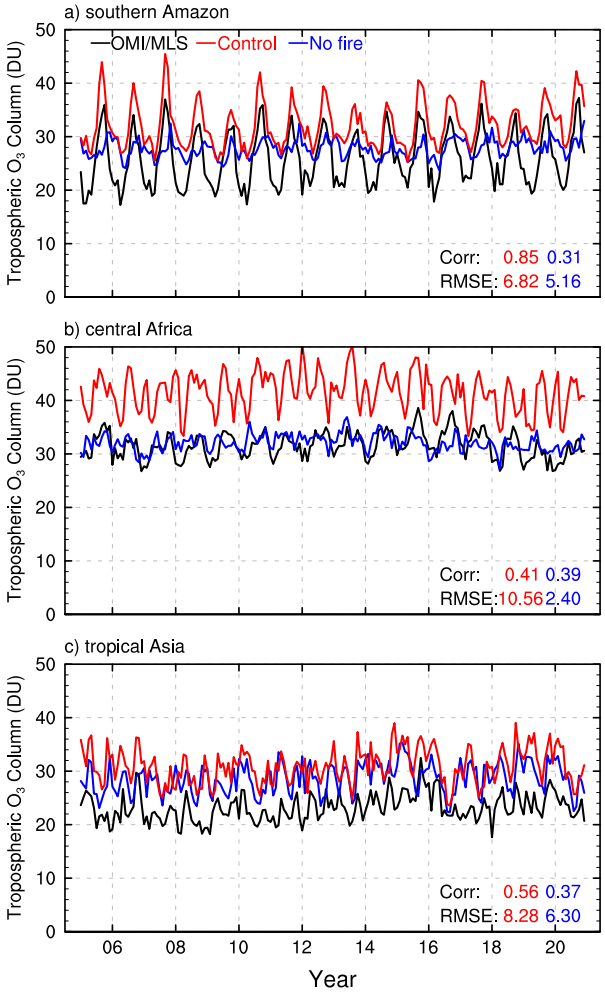

Figure 8: Time series of the OMI/MLS observed and modeled tropospheric O_3 column (DU) from the control (red line) and no-fire (blue line) simulations during 2005-2020 in a) southern Amazon, b) central Africa, and c) tropical Asia. The Pearson correlation and root mean square error (i.e., RMSE) between the modeled and observed values are given in each panel. The red and blue texts represent the computed values for the control and no-fire simulations, respectively.

https://doi.org/10.5194/egusphere-2026-4288
Preprint. Discussion started: 14 September 2026

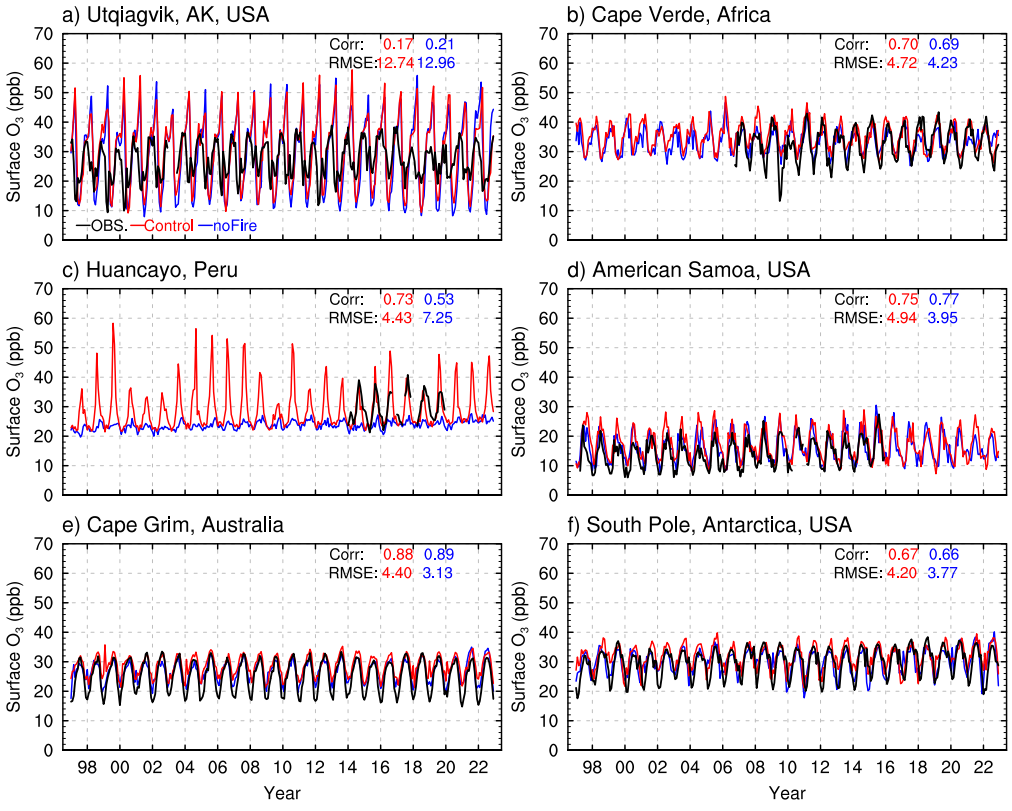

Figure 9: Time series of surface O_3 mole fractions (ppb) from in-situ observations (black line), the control (red line) and no-fire simulations (blue line) during 1997-2022 in a) Utqiaġvik, AK, USA (formerly Point Barrow), b) Cape Verde, Africa, c) Huancayo, Peru, d) American Samoa, USA, e) Cape Grim, Australia, f) South Pole, Antarctica, USA. The Pearson correlation and root mean square error (i.e., RMSE) between the modeled and observed values are given in each panel. The red and blue texts represent the computed values for the control and no-fire simulations, respectively.

https://doi.org/10.5194/egusphere-2026-4288
Preprint. Discussion started: 14 September 2026

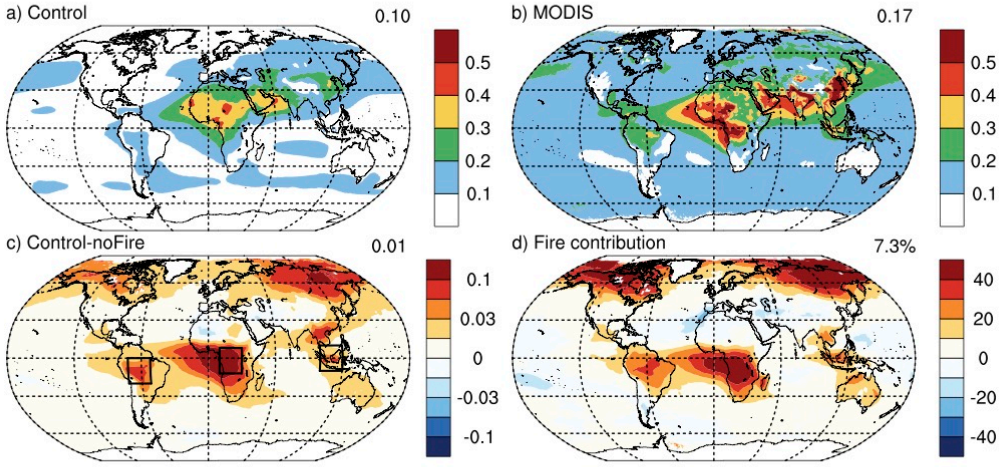

Figure 10: Annual mean aerosol optical depth (AOD) at 550 nm during February 2000-December 2022 for a) the control run, b) the MODIS satellite data, c) the absolute difference between the control and no-fire run, d) fire contribution in terms of the relative percentage difference (%) between the control and no-fire runs. The selected 20°×20° three tropical regions in the southern Amazon, central Africa and tropical Asia are marked with black squares. The global area-weighted mean values are shown in the upper right corner of each panel.

https://doi.org/10.5194/egusphere-2026-4288
Preprint. Discussion started: 14 September 2026

1194
1195

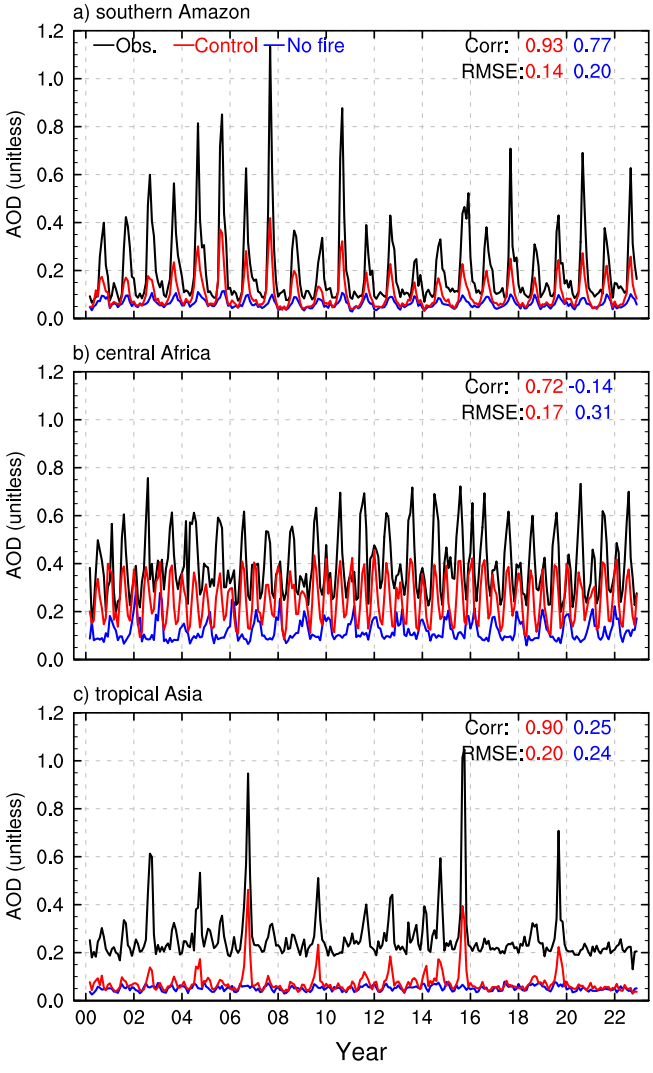

Figure 11: Time series of the MODIS observed and modeled aerosol optical depth (unitless) from the control (red line) and no-fire (blue line) simulations during February 2000-December 2022 in a) Southern Amazon, b) Central Africa, and c) Tropical Asia. The correlation and root mean square error (i.e., RMSE) between the modeled and observed values are given in each panel. The red and blue texts represent the computed values for the control and no-fire simulations, respectively.

https://doi.org/10.5194/egusphere-2026-4288
Preprint. Discussion started: 14 September 2026

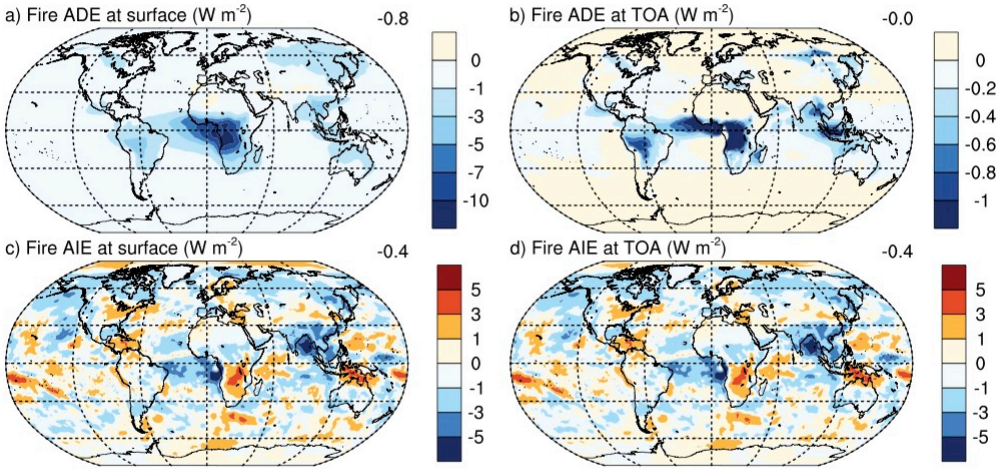

Figure 12: Annual average simulated a) fire aerosol direct effect (ADE) at surface (W m^{-2}), b) fire aerosol direct effect at the top of atmosphere (TOA) (W m^{-2}), c) fire aerosol indirect effect (AIE) at surface (W m^{-2}), d) fire aerosol indirect effect at the top of atmosphere (TOA) (W m^{-2}) during 1997-2022. The global area-weighted mean values are shown in upper right corner of each panel.

https://doi.org/10.5194/egusphere-2026-4288
Preprint. Discussion started: 14 September 2026

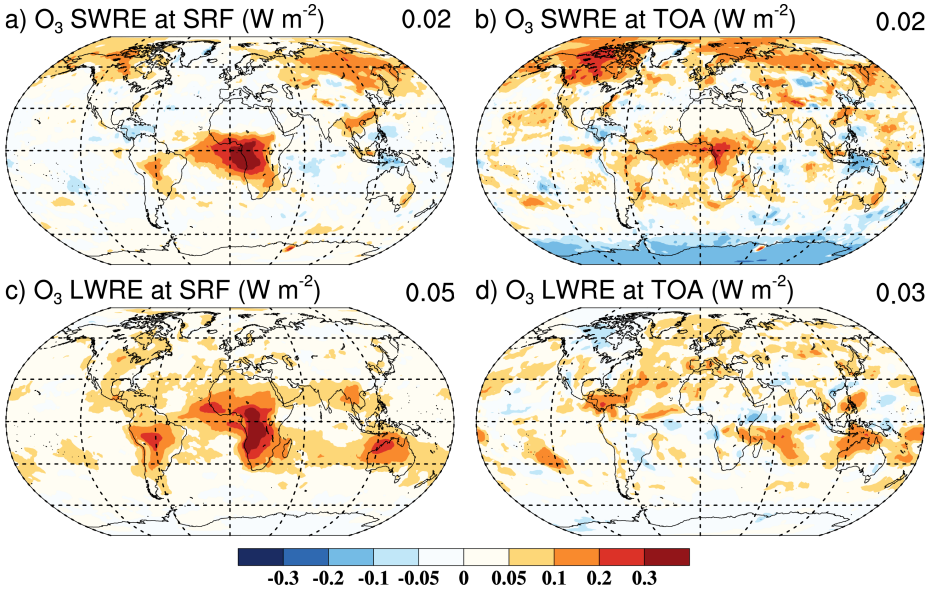

Figure 13: Annual average simulated fire-induced a) O_3 shortwave radiative effect (SWRE) at surface (W m^{-2}), b) O_3 shortwave radiative effect at the top of atmosphere (TOA) (W m^{-2}), c) O_3 longwave radiative effect (LWRE) at surface (W m^{-2}), d) O_3 longwave radiative effect at the top of atmosphere (W m^{-2}) during 1997-2022. The fire-induced radiative effects were calculated as the difference in radiative flux of O_3 between the control and no-fire simulations. The global area-weighted mean values are shown in upper right corner of each panel.

https://doi.org/10.5194/egusphere-2026-4288
Preprint. Discussion started: 14 September 2026

Table 1: Numerical experiments used in this study.

Experiment	Description
Control	Include all direct emissions for trace gases and aerosols
No fire	Exclude fire emissions for trace gases and aerosols

Table 2: Annual mean fire emissions of trace gases and aerosols from 1997-2022 used in this study and their relative contribution to total emissions from all sources. Standard deviations are derived from year-to-year variability in emissions and do not capture the full range of uncertainty stemming from biomass emissions and emission factor estimates.

Species[a]	Fire Emissions (Tg species y^{-1})	Fire relative contribution (%)
CO	529.7±74.2	46.5±3.1
C_2H_4	7.4±0.7	16.7±1.4
C_2H_6	5.4±0.7	48.3±3.6
C_3H_8	1.9±0.9	25.2±7.7
CH_2O	9.9±0.9	59.8±2.2
CH_3CHO	11.9±1.0	37.0±2.0
CH_3COCH_3	3.5±0.4	8.3±0.8
Isoprene	1.0±0.2	0.2±0.0
Monoterpene	4.6±1.0	4.6±0.8
NO	24.3±1.8	22.1±1.5
SO_2	5.9±0.6	4.6±0.7
SOAG0	57.0±7.7	68.0±3.2
BC	2.5±0.2	37.1±2.0
POM	38.0±5.1	72.7±2.6

[a]Annual CH_4 emissions from GFED5 are estimated to be18.7 ± 3.4 Tg CH_4 y^{-1}. These emissions were not included in this work because CH_4 tracer is not implemented as a fully interactive tracer in the current model version.

https://doi.org/10.5194/egusphere-2026-4288
Preprint. Discussion started: 14 September 2026

Table 3: Correlations between E3SM simulations and observations for the annual mean spatial pattern, a monthly climatological annual cycle, monthly anomalies (IAV only) and the full time series. For CO, the model was compared with MOPITT column observations, for O_3 the model was compared with OMI/MLS column observations, and for aerosol optical depth (AOD), the model was compared with MODIS observations.

Species	Simulations	Annual mean (180°×360°)	Annual cycle (12m×180°×360°)	IAV only (276m×180°×360°)[a]	Full time series (276m×180°×360°)[a]
CO	Control	0.88	0.85	0.45	0.80
	No fire	0.75	0.61	-0.24	0.52
O_3	Control	0.69	0.70	0.26	0.62
	No fire	0.75	0.72	0.19	0.63
AOD	Control	0.75	0.70	0.19	0.60
	No fire	0.65	0.60	0.07	0.49

[a]The total time dimension for the CO and AOD modeled data and measurements during 2000-2022 is 276 months (i.e., 23 years) while that for O_3 data during 2005-2020 is 192 months (i.e., 16 years).

Table 4: Pearson correlation (r) and root mean square error (RMSE) for the time series of the regional average modeled CO column and MOPITT CO column shown in Figure 5, the regional modeled tropospheric O_3 column and OMI/MLS O_3 column shown in Figure 8, and the regional modeled aerosol optical depth (AOD) and MODIS data shown in Figure 11 in Southern Amazon, Central Africa and Tropical Asia. The modeled CO column, O_3 column and AOD from both control and no fire simulations are reported.

Variable	Simulations	Regions					
		Southern Amazon		Central Africa		Tropical Asia	
		r	RMSE	r	RMSE	r	RMSE
CO	Control	0.93	2.53	0.83	3.15	0.84	2.09
	No fire	0.46	5.27	-0.07	8.13	-0.02	5.26
O_3	Control	0.85	6.82	0.41	10.56	0.56	8.28
	No Fire	0.31	5.16	0.39	2.40	0.37	6.30
AOD	Control	0.93	0.14	0.72	0.17	0.90	0.20
	No fire	0.77	0.20	-0.14	0.31	0.25	0.24